

## The Canada-UK Deep Submillimeter Survey: IV. The Survey of the 14-Hour Field

Stephen Eales<sup>1</sup>, Simon Lilly<sup>2</sup>, Tracy Webb<sup>2</sup>, Loretta Dunne<sup>1</sup>, Walter Gear<sup>1</sup>, David Clements<sup>1</sup> and Min Yun<sup>3</sup>

### ABSTRACT

We have used SCUBA to survey an area of  $\simeq 50$  arcmin $^2$ , detecting 19 sources down to a  $3\sigma$  sensitivity limit of  $\sim 3.5$  mJy at 850 $\mu$ m. Monte-Carlo simulations have shown that the fluxes of sources in this and similar SCUBA surveys are biased upwards by the effects of source confusion and noise, leading to an overestimate by a factor of  $\sim 1.4$  in the fraction of the 850 $\mu$ m background that has been resolved by SCUBA. Once a correction is made for this effect, about 20% of the background has been resolved. The simulations have also been used to quantify the effects of confusion on source positions. Of the 19 SCUBA sources, five are  $\mu$ Jy radio sources and two are ISO 15 $\mu$ m sources. The radio/submillimetre flux ratios imply that the dust in these galaxies is being heated by young stars rather than AGN. The upper limit to the average 450 $\mu$ m/850 $\mu$ m flux ratio implies either that the SCUBA galaxies are at  $z >> 2$  or, if they are at lower redshifts, that the dust is generally colder than in ULIRGs.

We have used simple evolution models to address the major questions about the SCUBA sources: (1) what fraction of the star formation at high redshift is hidden by dust? (2) Does the submillimetre luminosity density reach a maximum at some redshift? (3) If the SCUBA sources are proto-ellipticals, when exactly did ellipticals form? We show, however, that the observations are not yet good enough to answer these questions. There are, for example, acceptable models in which 10 times as much high-redshift star formation is hidden by dust as is seen at optical wavelengths, but also acceptable ones in which the amount of hidden star formation is less than that seen optically. There are also acceptable models in which very little star formation occurred before a redshift of three (as might be expected in models of hierarchical galaxy formation), but also ones in which 30% of the stars have formed by this redshift. The key to answering these questions are measurements of the dust temperatures and redshifts of the SCUBA sources.

*Subject headings:* galaxies: evolution — galaxies: formation — infrared: galaxies — cosmology: observations — surveys

---

<sup>1</sup>Department of Physics and Astronomy, Cardiff University, P.O. Box 913, Cardiff CF2 3YB, UK

<sup>2</sup>Department of Astronomy, University of Toronto, 60 St. George Street, Toronto, Ontario M5S 1A1, Canada

<sup>3</sup>National Radio Astronomy Observatory, P.O. Box 0, 1003 Lopezville Road, Socorro, NM 87801

## 1. Introduction

The extragalactic background contains all the energy ever emitted by galaxies, with the radiation from galaxies at a redshift  $z$  being weighted by a factor  $(1+z)^{-1}$ . Thus determining the level of the background in different wavebands and resolving the background into individual sources is of great importance for determining the history of the energy output of galaxies. Recent measurements suggest that (setting aside the cosmic microwave-background radiation from the very early universe) the extragalactic background is dominated by emission in two spectral regions, the optical/near-infrared and the submillimetre wavebands ( $100\mu\text{m} < \lambda < 1\text{mm}$ ), with roughly equal integrated emission in the two wavebands (Dwek et al. 1998). The spectral shape of the background emission in the submillimetre waveband is characteristic of dust emission spread over a range of redshift (Puget et al. 1996; Lagache, Puget and Gispert 1999). Therefore, although there is some uncertainty from the  $(1+z)^{-1}$  weighting factor, this approximate equality suggests that half the energy ever directly emitted by stars and active galactic nuclei (AGN) has been absorbed by dust and then re-radiated at long wavelengths. Since young stars are generally more heavily obscured than old stars, the fraction of the universe's star formation that is hidden by dust may well be significantly greater than half. The only caveat to these arguments is if there is some more exotic population of objects dominating the submillimetre background (Bond, Carr & Hogan 1986, 1991).

If the extragalactic background is dominated by stars, the history of the energy output of galaxies is closely linked to the history of star formation in the universe. The background radiation and the local properties of galaxies give complementary information about this history. Consider the problem of the origin of elliptical galaxies and spiral bulges. The stars in nearby ellipticals and spiral bulges are often extremely old (Bower, Lucey & Ellis 1992), implying that much of the star formation in these objects must have occurred at very early times. Ellipticals and spiral bulges in this initial star-forming phase should be very luminous, yet optical surveys have failed to find convincing evidence of such “proto-spheroids” (De Propris et al. 1993). However, these objects must make a major contribution to the extragalactic background radiation. The relation between the integrated background emission produced by a population at a redshift  $z$  and the average cosmic density of processed material,  $\langle \rho(Z + \Delta Y) \rangle$ , produced by this population is:

$$\int_0^\infty I_\nu d\nu = \frac{0.007 \langle \rho(Z + \Delta Y) \rangle c^3}{4\pi(1+z)}, \quad (1)$$

(Pagel 1997). Given the quantity of metals associated with nearby ellipticals (Edmunds and Phillipps 1997), this relation implies that ellipticals in their rapid star-forming phase should be responsible for about half the background radiation. Thus resolving the extragalactic background into individual sources *must* solve this problem.

The measurement of the integrated optical background recently made by Bernstein and col-

laborators (Bernstein 1999) is only about twice that obtained by simply adding up the emission in deep galaxy counts (Williams et al. 1996) and indeed Bernstein argues that the integrated optical background can be explained by known populations of objects. Thus the optical background may already have been completely resolved and no obvious proto-spheroids have been found. For example, the galaxies at  $z \sim 3$  found by the Lyman-break technique (Steidel et al. 1999) contribute  $\sim 2\%$  of the background in the I-band and thus, by the metallicity argument above, are unlikely to be the missing proto-spheroids. This apparent failure to find proto-spheroids at optical wavelengths, together with the metallicity argument, suggests that proto-spheroids must dominate the other important component of the background at submillimetre wavelengths. A physical explanation of this would be if the initial formation of stars in the spheroids leads to the rapid creation of dust, which then absorbs the optical/UV radiation (Eales and Edmunds 1996; Eales and Edmunds 1997).

Resolving the submillimetre background radiation into individual sources is thus of great interest. It has recently become possible to do this, at least partially, with the ISOPHOT instrument on the Infrared Space Observatory at short wavelengths and with the SCUBA submillimeter array (Holland et al. 1999) on the James Clerk Maxwell Telescope (JCMT) at long wavelengths. This paper is the fourth of a series of papers describing the results of a deep submillimetre survey with SCUBA (Eales et al. 1999; Lilly et al. 1999—henceforth Papers I and II). Before describing the scope of the present paper, we will briefly summarize the results of our and other submillimetre surveys.

The ISOPHOT surveys are important because the submillimetre background radiation peaks at short wavelengths, and thus, in energy terms, it is more important to resolve the background here than at the longer wavelengths sampled by SCUBA. Surveys with ISOPHOT have found sources that contribute about 10% of the submillimetre background at  $175 \mu\text{m}$  (Kawara et al. 1998; Puget et al. 1999). However, the large size of the ISOPHOT beam (1.9 arcmin, full-width half-maximum) means that it is remarkably difficult to identify the galaxies responsible for the submillimetre emission (Scott et al. 2000).

The main operating wavelength of SCUBA is  $850\mu\text{m}$ , where the submillimetre background is much lower than at its peak ( $\nu I_\nu$  lower by a factor of  $\sim 30$ ), but SCUBA has the great advantage over ISOPHOT that its much smaller beamsize (14 arcsec, full-width half-maximum) means that it is possible (although still difficult) to identify the galaxies responsible for the submillimetre emission. SCUBA has been used to investigate the high-redshift universe through three different methods. The first is to obtain submillimetre images in the directions of rich clusters, thus using the lensing effect of the clusters both to amplify the submillimetre fluxes of high-redshift submillimetre sources and to reduce the effect of source confusion (Smail, Ivison & Blain 1997; Smail et al. 1998; Blain et al. 1999b). The disadvantages of this are the need to separate background from cluster sources and for an accurate lensing model for each cluster. The second method is to carry out truly ‘blind-field’ submillimetre surveys, which do not have the disadvantages of the cluster method but at the expense of greater problems with confusion and much longer integration times to get to the same effective sensitivity. The deepest blind survey that has so far been carried out is a survey of the

Hubble Deep Field (Hughes et al. 1998). Our survey, which is not so deep but which covers a wider area, is also of fields which have been extensively surveyed at other wavelengths: the Canada-France Redshift Survey fields (CFRS; Lilly et al. 1995). The Hawaii group has been carrying out a survey with a similar depth to our own (Barger et al. 1998; Barger, Cowie & Sanders 1999). The third of the methods is to carry out SCUBA observations of known high-redshift objects. This will be discussed below but we will first summarize the scientific results of the surveys.

It has been claimed (Blain et al. 1999b,c) that the SCUBA surveys have resolved close to 100% of the background at  $850\mu\text{m}$ , although we will argue in this paper that this is an overestimate. Despite controversy over the details of which galaxies are responsible for the submillimetre emission, caused by the large positional errors of SCUBA, all the teams carrying out SCUBA surveys agree that these galaxies are similar to the ultra-luminous infrared galaxies (ULIRG's; Sanders & Mirabel 1996) found in the local universe (Hughes et al. 1998; Barger et al. 1998; Lilly et al. 1999; Smail et al. 1998). From these two results one can draw an extremely important conclusion (Paper I). If ULIRG's make up  $>50\%$  of the submillimetre background, they must constitute  $>\simeq25\%$  of the total extragalactic background radiation; and thus, as long as the dust in ULIRG's is heated by stars rather than AGN, roughly one quarter of all the stars that have ever formed must have formed in extreme systems like this rather than in normal galaxies like our own. This fact, together with the extreme bolometric luminosities of ULIRG's, which imply star-formation rates of  $10^2 - 10^3 \text{ M}_\odot \text{ year}^{-1}$  (Rieke et al. 1985), make it difficult to avoid the conclusion that these systems are proto-spheroids.

Hughes et al. (1998) and Barger, Cowie and Richards (2000) have also argued that the results of the SCUBA surveys and the strength of the submillimetre background imply the amount of star formation hidden by dust in the early universe is an order of magnitude greater than that seen directly in optical surveys—in effect that the universe had a ‘Dark Age’ in which the fraction of star formation hidden by dust was much greater than it is today. In our earlier work, we found little evidence for this, concluding that the cosmic evolution seen in the submillimetre waveband is similar to that seen at optical wavelengths and thus that the fraction of young stars hidden by dust is the same at all cosmic epochs (Paper I). Moreover, the fraction of the SCUBA sources identified with galaxies at  $z < 1$  suggested that the submillimetre luminosity-density declines at  $z > 2$  (Paper II), which is where the other studies claim the majority of the dust emission is occurring. We will revisit this question in this paper.

There are two fundamental uncertainties in the conclusions above. The first of these is simply the sensitivity of these conclusions to dust temperature, which for the SCUBA sources is largely unknown. Up to  $z \sim 3$ , the main SCUBA operating wavelength of  $850\mu\text{m}$  falls, in the rest frame, on the Rayleigh-Jeans side of the typical dust spectral energy distribution, and thus dust temperature is critical for calculating the total dust luminosity; for a dust source with a dust emissivity index of two, the total dust emission is proportional to the dust temperature to the sixth power, and thus an uncertainty of a factor of two in dust temperature leads to an uncertainty of a factor of 64 in total luminosity. This uncertainty holds for both individual sources and for the population of SCUBA

sources as a whole. Even the conclusion that a SCUBA galaxy is essentially a ULIRG is affected. Fig. 1 shows the bolometric luminosity calculated for a SCUBA source with  $S_{850\mu\text{m}} = 4\text{mJy}$  as a function of redshift and for a number of assumed dust temperatures. Also shown is the bolometric luminosity of the archetypical ULIRG Arp 220. If instead of assuming a dust temperature typical of a ULIRG, for which there is rarely any observational justification, one assumes a dust temperature typical of a normal spiral galaxy, one obtains a bolometric luminosity an order-of-magnitude lower than that of Arp 220. Thus, the argument that the estimated bolometric luminosities imply SCUBA galaxies are ULIRGs is circular: if one assumes the dust temperature typical of a ULIRG, one necessarily obtains the bolometric luminosity of a ULIRG. We will explore the importance of this uncertainty for the population as a whole later in this paper.

The second of the uncertainties is whether the dust in a SCUBA galaxy is actually being heated by young stars or whether it is being heated by an obscured active galactic nucleus (AGN); if it is the latter, of course, then the conclusion that the SCUBA galaxies are proto-ellipticals is completely wrong. Two results suggest that the AGN hypothesis may be the correct one. First, the recent discovery that there are black holes in the centres of most nearby galaxies (Magorrian et al. 1998) suggests that most galaxies have passed through a phase in which they harboured an active nucleus, implying in turn that AGN might contribute a significant fraction of the extragalactic background radiation. Estimating the exact fraction of the total extragalactic background emission that is produced by AGN is difficult, mainly because one does not know how efficiently mass was turned into radiation as the black hole formed (Haehnelt, Natarajan and Rees 1998), and even simple estimates range from 10% (Eales et al. 1999) to 60% (Lilly, unpublished). Second, it has been known for a long time (Setti & Woltjer 1989) that one way of explaining the spectral dependence of the X-ray background is by a new population of highly obscured AGN, and the submillimetre waveband would be the natural place for the absorbed emission to reappear.

Settling this issue is unfortunately difficult. Although the evidence from mid-infrared line ratios (Genzel et al. 1998; Lutz et al. 1998) and from VLBI radio observations (Smith et al. 1998) is that stars rather than AGN are the main energy source in low-redshift ULIRGs, it is not possible to use these techniques for the SCUBA galaxies. One result that does suggest that this is also the case for the SCUBA galaxies is that they are often detected in very deep radio surveys with ratios of dust to radio emission similar to those seen in samples of nearby star-forming galaxies (Lilly et al. 1999; Barger, Cowie & Richards 2000). Barger et al., for example, found that five of the seven sources detected in a SCUBA survey of the Hubble Flanking Fields were detected in the radio survey of the same region. One way of addressing the possibility that the SCUBA galaxies are the obscured AGN needed to explain the X-ray background would be deep X-ray surveys of fields surveyed with SCUBA, something now possible with Chandra and Newton. The first of these surveys (Fabian et al. 2000; Hornschemeier et al. 2000) suggest that it is young stars rather than AGN heating the dust.

The third of the methods used to investigate the high-redshift universe with SCUBA has been to use SCUBA to observe known classes of object. Observations of samples of high-redshift radio

galaxies have shown that the average submillimetre luminosity of these objects rise as  $(1 + z)^3$  out to  $z \sim 4$  (Archibald et al. 2000), very different from the ways in which the luminosity-density of the galaxy population as a whole is inferred to evolve, either from optical (Steidel et al. 1999) or submillimetre (Blain et al. 1999a; Eales et al. 1999; Lilly et al. 1999) observations. SCUBA observations have also been carried out of the high-redshift galaxies found using the Lyman-break technique (Steidel et al. 1999). Observations of individual galaxies have resulted in only a single detection (Chapman et al. 2000), but Peacock et al. (2000) have claimed a statistical detection of the population by summing the submillimetre emission at the positions of Lyman-break galaxies in the deep SCUBA image of the Hubble Deep Field. This has implications for whether the Lyman-break galaxies and the galaxies found in the deep SCUBA surveys are distinct populations. They can not be completely separate, of course, because any SCUBA galaxy at the right redshift will necessarily have a Lyman break in its *UV* spectrum; the question is really whether, as Adelberger and Steidel (2000) have recently claimed, one can learn all one needs to know about high-redshift galaxies by studying the Lyman-break population and making the necessary bolometric corrections for each galaxy to allow for the dust emission. However, the optical/IR observations of the SCUBA sources suggest that this is not correct, because even the brightest SCUBA sources frequently have optical counterparts that are too faint to have been detected in any of the optical searches for Lyman-break galaxies (e.g. Gear et al. 2000). We will investigate this question in more detail later in this paper.

In Paper I of this series (Eales et al. 1999) we described submillimetre observations of three fields: two small fields within the CFRS  $3^h$  and  $10^h$  fields and a larger field within the CFRS  $14^h$  field. Paper II (Lilly et al. 1999) considered the optical, radio and mid-infrared properties of these fields in an attempt to identify and determine the properties of the galaxies responsible for the submillimetre emission. Paper III (Gear et al. 2000) describes interferometry at millimetre wavelengths and deep optical/IR imaging and spectroscopy of the brightest SCUBA source in the  $14^h$  field. After our initial observations of the two small fields, our strategy changed to a systematic attempt to map at submillimetre wavelengths as great a fraction as possible of the CFRS  $3^h$  and  $14^h$  fields, which are the two with ISO mid-infrared images. In this paper we report the results of our submillimetre survey of the  $14^h$  field and compare the submillimetre, radio and mid-infrared results, in an attempt to understand the properties of the SCUBA galaxy population. Subsequent papers will describe the optical and near-infrared properties of this field and also the results of the survey of the  $3^h$  field.

In this paper we will use the results of another survey, the SCUBA Local Universe Galaxy Survey (SLUGS; Dunne et al. 2000). This is a parallel submillimetre survey of the local universe meant to serve as a zero-redshift benchmark against which the surveys of the high-redshift universe can be compared. Dunne et al. have recently published the first estimate of the local  $850\mu\text{m}$  luminosity function based on SCUBA observations of a sample of 104 galaxies selected from the IRAS Bright Galaxy Sample (Soifer et al. 1989). We will use this luminosity function and a number of other results from SLUGS later in this paper.

The arrangement of this paper is as follows. Sections 2 and 3 describe the observations and the data reduction. Section 4 describes how a catalog of sources was selected from the final image and includes a detailed investigation of the reliability of the catalog which is applicable to all SCUBA surveys. Section 5 describes a search for associations of SCUBA sources with mid-infrared and radio sources. Section 6 contains a discussion of the results of the current survey and includes an estimate of the redshift distribution. Section 7 describes detailed modelling of the SCUBA galaxy population and a discussion of its cosmological significance. We everywhere assume a Hubble Constant of  $75 \text{ km s}^{-1} \text{ Mpc}^{-1}$ .

## 2. Observations

We observed the  $14^h$  field with SCUBA on 20 nights between 1998 March 5 and 1999 May 27. SCUBA is described in detail elsewhere (Holland et al. 1999) but, briefly, it consists of 91 bolometers for observations at short wavelengths, usually  $450 \mu\text{m}$ , and 37 bolometers for observations at long wavelengths, usually  $850 \mu\text{m}$ ; a dichroic beamsplitter is used to simultaneously observe the same field at the two wavelengths. The field-of-view of the array is roughly circular with a diameter of about 2.3 arcmin. The beam size is about 8 arcsec and 14 arcsec (full-width half-maximum) at  $450$  and  $850 \mu\text{m}$ . As the bolometers in the array do not fully-sample the sky, the secondary mirror is moved in a hexagonal pattern, producing a fully-sampled image known as a ‘jiggle map’ (Holland et al. 1999). SCUBA sits at the Nasmyth focus of the JCMT (i.e. fixed relative to the Earth) so each bolometer gradually moves in a circular path around the field centre.

For our observations we used a 64-point jiggle pattern, which produces fully-sampled maps at both wavelengths. As in classical infrared and submillimetre astronomy, we chopped and nodded the JCMT secondary mirror to remove temporal fluctuations and linear spatial gradients in the sky brightness, using a ‘chop throw’ of 30 arcsec in Right Ascension. This small angle, only twice the size of the JCMT beam, maximizes the accuracy of the sky removal and also means that a source is likely to remain on the array even when the array is centered at the reference position, increasing the effective integration time on the source. This does, however, introduce the complication that any real source will appear as a positive peak with negative peaks of half the amplitude 30 arcsec to the east and west of the positive peak. The individual units of our survey were jiggle-map observations at a number of field centres within the overall survey region. Each observation lasted about one hour. The field centres were chosen with the aim of producing a map with uniform noise. Each point in the final map incorporates data from a large number of separate datasets (typically nine) and from a large number of different bolometers, since the bolometers move with respect to the sky. This lessens the chance of problems with individual bolometers generating spurious sources.

Before each individual observation we checked the pointing of the telescope on a nearby JCMT pointing source. During each night we monitored the opacity of the atmosphere at both  $450$  and  $850 \mu\text{m}$  using ‘skydips’ and we determined the flux calibration from observations of one or more

of the following calibrators: Mars, Uranus, CRL618, IRC+10216. The photometric accuracy of SCUBA observations at  $850\text{ }\mu\text{m}$  is remarkably good and we estimate that the basic photometric uncertainty (i.e. the flux error for an object with infinite signal-to-noise) is only  $\simeq 5\%$ ; at  $450\text{ }\mu\text{m}$  it is rather worse,  $\simeq 20\%$ , because the flux calibration is much more sensitive at this wavelength to errors in the dish surface, which depend strongly on the recent thermal history of the dish.

Details of the nights on which we observed are given in Table 1.

### 3. Data Reduction

We reduced the data independently in Cardiff and Toronto using the SURF package (Jenness 1997) in the following way. First, for each bolometer we subtracted the intensity measured at the reference position from the intensity measured at the target position, dividing the result by the array's flat-field to correct for sensitivity variations between bolometers. We then corrected each second of data for each bolometer for the atmospheric opacity at that time. After these standard steps we then inspected intensity versus time plots for each bolometer and excised obviously bad data, also running several SURF clipping routines which automatically flag bad data. Because of the jiggling technique, each point on the final map is made from data taken at a slightly different time, and thus a varying sky level can lead to increased noise on the final map. To avoid this, we ran the SURF program REMSKY, which subtracts from the intensity measured by each bolometer the median of intensities measured by all the bolometers at that time. Even in the relatively good conditions in which most of the data were taken, this step always made a large improvement to the final maps. Finally, we made a map, incorporating the data for each bolometer in each survey unit with the optimum statistical weighting, and using a spatial linear weighting function to regrid the data onto a rectangular mesh.

The final Cardiff  $850\text{ }\mu\text{m}$  map is shown in Fig. 2 (the Toronto version is very similar; the  $450\text{ }\mu\text{m}$  map, which has much poorer sensitivity, will be considered later). An edge region containing artefacts, a well-known phenomenon of the SCUBA map-making process, has been removed from the map. The negative lobes of many of the sources can clearly be seen and in the case of the brightest source (bottom right-hand quadrant) the effects of an error in the telescope software can even be seen in the slight offset of the lobes from an East-West direction (Until August 1998 the telescope software was correctly translating the telescope chop direction into the telescope's natural altitude-azimuth coordinates at the beginning of each integration but was not updating this calculation during the integration, resulting in this small rotation. The detailed effect of this on each source is impractical to model, but our simple models show that the size of the effect is small enough that an assumption of no rotation leads to a negligible effect on the source catalog.).

We tried to improve our map in two ways. First, we tried a more sophisticated sky-removal algorithm than that used in the REMSKY program, in which each bolometer is assumed to see the same sky brightness, by instead assuming that the sky brightness is a linear function of position.

This algorithm made a significant improvement to SCUBA data taken for other projects in poor atmospheric conditions (Dunne et al. 2000) but made negligible improvement to the map in Fig. 2. Second, we carried out a Fourier Transform of the data for each individual bolometer to look for bad data. This proved to be quite instructive, since although most bolometers had white-noise spectra, some had spectra in which the power was much greater at high frequencies; and on re-examination of the data back in the time domain, these always proved to be bolometers where there was some sign that the signal was correlated with that in other bolometers (possibly due to inadequate shielding between the electronics associated with each bolometer). We tried drastic filtering of these bolometers in the frequency domain. However, when the data were transformed back into the time domain and a new map made, it was very similar to that in Fig. 2. This failure to improve the basic map does suggest, however, that its features are robust and are not the result of gradients in sky emission or of noisy bolometers.

## 4. The Catalog

### 4.1. Selecting the Sources

To generate a catalog there are three problems to overcome: how to use the information in the negative as well as the positive lobes of each source; how to determine the significance of the sources; how to combat the effects of source confusion.

As in Paper I, we solved the first problem by convolving the raw map with a template of what a real source should look like in the absence of noise (Phillips and Davies 1991). We used Uranus as the template. We averaged all the maps of Uranus, which we observed many times during the survey with the same chop throw as for the survey, to provide a master template and convolved this with the raw survey image. This implicitly makes the assumption that a real SCUBA source will not be significantly extended, but this is a reasonable assumption given the relative sizes of the SCUBA beam and of the optical structures of high-redshift galaxies.

To model the noise, vital for determining the significance of the sources, we started with the basic assumption that the noise on a bolometer is independent of the noise on every other bolometer. We then took each individual pointing of one hour duration (the survey unit), measured the standard deviation of the intensities for each bolometer, and replaced the real data with the output of a Gaussian random-number generator with the same standard deviation as the data. The real data does not have a precisely Gaussian form, mainly because of the effects of some of the SURF routines, principally the clipping routines and REMSKY. So we ran the same SURF programs on the artificial data, and then rescaled the artificial data so that it had again the same standard deviation as the real data. In this way the histogram of intensities for an artificial bolometer is almost identical to that for the real data. We did the same for each bolometer within each survey unit, and then made a map with the artificial datasets, repeating this whole procedure until we had 1000 artificial maps. Since our source-selection procedure uses the real map convolved with

the template, we convolved the artificial maps with the same template. Fig. 2 shows the noise map produced by measuring the standard deviation of these convolved maps, pixel by pixel. As one would expect, the noise is a strong function of position. In particular, the noise in the upper third of the map is significantly worse than the noise elsewhere, because part of the image was made with data taken in May 1999, during which the atmospheric conditions were significantly worse than for the rest of the survey. The noise estimated from the deep area of the noise map is 0.94 mJy, whereas the noise on the real map after it has been convolved with the template and after all the significant sources have been subtracted (see below) is 0.90 mJy. These are remarkably similar, especially as the real map should contain a noise component due to faint sources below the sensitivity limit of our catalog.

The starting point for the catalog selection was the raw image convolved with the template and then divided by the noise image. This image is a map of signal-to-noise over the field. To address the problem of confusion we used the CLEAN algorithm. We first used the signal-to-noise map to produce a list of possible sources. We then iteratively CLEANed the *raw* map in boxes centred on the positions of these possible sources. Then, for each source in the list of possible sources, we adopted the following procedure. First, use the information from CLEAN to remove all other possible sources from the raw map. Then convolve this new map with the source template and divide the convolved map by the noise map, and so measure the signal-to-noise of the possible source. In this way, we generated a catalog of sources, producing (as in Paper I) fluxes and positions from the template-convolved map, the optimum procedure for measuring fluxes and positions (Phillips and Davies 1991).

An important question is the minimum signal-to-noise a source should have to be included in the catalog. As in Paper I, we adopted the pragmatic solution of carrying out exactly the same selection procedure on the negative of the map, to determine the number of spurious sources as a function of signal-to-noise. We adopted a minimum signal-to-noise of three, since this is the point at which the ratio of spurious to real sources starts to climb sharply.

We independently carried out this procedure on the Cardiff and Toronto maps and Table 2 contains the sources that met the  $3\sigma$  threshold in both catalogs. The positions and fluxes are the averages of the values for the two catalogs. There are 19 sources in the catalogue. Undoubtedly a small number are spurious. We will address this whole problem in more detail in the next section, but a simple argument suggests that 2-3 are probably false detections. First, applying the selection procedure to the negative map resulted in two detections, both at  $\simeq 3\sigma$ . Second, given the number of beam areas in our survey area, Gaussian statistics imply that a  $3\sigma$  cutoff should produce 2.6 spurious sources.

Of the seven sources in this field listed in Paper I, three now fall outside the sample. One of these, CFRS 14G, was right at the edge of the region we thought free of edge artefacts but is clearly such an artefact. The other two are still detected (their new fluxes and positions are given in Table 3) but at a level below the nominal catalog limit. This loss of sources is of course expected. If

sources are close to the signal-to-noise limit of a sample, a small amount of new data will result in approximately as many sources being lost from the catalog as are gained.

We measured 450  $\mu\text{m}$  fluxes for the 850  $\mu\text{m}$  sources by aperture photometry with an aperture of diameter 12 arcsec centered on the 850  $\mu\text{m}$  position, using the technique of Dunne et al. (2000) to obtain the errors. Only one source is detected at  $>2\sigma$  (Table 2). It is possible that even if individual sources are not detected at a significant level, the population as a whole is. We tested this by making a weighted average of the 450  $\mu\text{m}$  flux densities in Table 2 (excluding the two most inaccurate values which are for objects right at the edge of the slightly smaller 450  $\mu\text{m}$  map and so are probably unreliable). We obtained  $\langle S_{450\mu\text{m}} \rangle = 2.2 \pm 2.7 \text{ mJy}$  and thus did not obtain a significant detection. The corresponding weighted average at 850  $\mu\text{m}$  is  $\langle S_{850\mu\text{m}} \rangle = 4.34 \pm 0.46 \text{ mJy}$ . This result will be discussed further in §6.

Fig. 3 shows the raw source counts with a correction made for the sensitivity variation over the image but none made for the effect of flux errors. These agree fairly well with those of other surveys (Hughes et al. 1998; Barger, Cowie & Sanders 1999; Blain et al. 1999b). We examine the effects of incompleteness and confusion on the sources counts in §4.3.

#### 4.2. Notes on Individual Sources

In this section we give notes on individual sources. The positional accuracy of the SCUBA sources is important for determining the optical/IR counterparts. Since we independently reduced the data and compiled catalogs in Cardiff and Toronto, one partial check on the accuracy is whether the Cardiff and Toronto positions agree. We give below the positional disagreements of all sources for which the disagreement is  $>2$  arcsec and also note sources which are particularly close to each other.

**CUDSS 14.1:** This source is the brightest source in our survey of the 14-hour field. It is only 0.9 arcsec away from a  $\mu\text{Jy}$  radio source, with which it is clearly associated (§5.2). In Paper II we showed that the optical/IR counterpart to this submillimetre/radio source is a faint red galaxy with  $K_{\text{AB}} \simeq 21$ . Millimetre interferometry, which confirms the identification proposed in Paper II, and deep optical/IR imaging and spectroscopy of this source are described in Paper III (Gear et al. 2000).

**CUDSS 14.2:** This is the second brightest of the sources in the 14-hour field. In Paper II we found a possible optical counterpart, although the probability of this being a chance coincidence was quite high. The new submillimetre position is further away from the optical position, increasing the probability that the two objects are unrelated. In this case there is no radio source to help determine the optical/IR counterpart.

**CUDSS 14.3:** This source is 2.7 arcsec away from a  $\mu\text{Jy}$  radio source, with which it is clearly associated (§5.2).

**CUDSS 14.4:** This is close to CUDSS 14.13 and this pair of sources is one of the two worst cases of confusion in the survey, the other being the pair 14.7/14.10. However, the Cardiff and Toronto positions for 14.4 are in good agreement.

**CUDSS 14.5:** This is close to CUDSS 14.9, but the two positions agree well.

**CUDSS 14.7:** This is close to CUDSS 14.10 and this pair of sources is one of the two worst cases of confusion in the survey, the other being the pair 14.4/14.13. However, the Cardiff and Toronto positions for 14.7 are in good agreement.

**CUDSS 14.8:** The Cardiff and Toronto positions disagreed by 2.8 arcsec for no obvious reason.

**CUDSS 14.9:** This is close to CUDSS 14.5, but the SCUBA position is only one arcsec from a radio source (§5.2), showing that the SCUBA position is accurate.

**CUDSS 14.10:** This is close to CUDSS 14.7 and this pair of sources is one of the two worst cases of confusion in the survey, the other being the pair 14.4/14.13. However, the Cardiff and Toronto positions for 14.10 are in good agreement.

**CUDSS 14.13:** This is close to CUDSS 14.4 and this pair of sources is one of the two worst cases of confusion in the survey, the other being the pair 14.7/14.10. The Cardiff and Toronto positions agree well, but in this case there is a galaxy 5.9 arcsec away from the SCUBA position which is a radio source and ISO source (§5) and which has a very disturbed optical structure (as shown by HST imaging). As a statistical argument (§5) shows that the chance of this galaxy not being the counterpart to the SCUBA source is low, as this is one of the two worst cases of confusion, and as the investigation of the effects of confusion (§4.3) shows that offsets this large will happen in  $\simeq 10\%$  of cases, we conclude that the SCUBA position is wrong by this amount. The redshift of the galaxy is 1.15.

**CUDSS 14.17:** The Cardiff and Toronto positions disagree by 5.3 arcsec, indicating that the position in Table 2 is quite inaccurate. This is probably caused by the source being close to the edge of the field, where the noise is varying rapidly with position. This source is 10.3 arcsec away from an ISO  $15\mu\text{m}$  source (§5), and although we would not consider it likely that the ISO galaxy is associated with the SCUBA source, the large disagreement between the two SCUBA positions makes it at least possible.

**CUDSS 14.18:** This source is 2.0 arcsec away from a  $\mu\text{Jy}$  radio source (§5.2) and an ISO source (§5.1). The probabilities of these being chance coincidences are very low. The redshift of the galaxy associated with the radio/ISO/SCUBA source is 0.66.

**CUDSS 14.19:** The Cardiff and Toronto positions disagree by 4.5 arcsec, indicating that the position in Table 2 is quite inaccurate. This is probably caused by the source being close to the edge of the field, where the noise is varying rapidly with position.

### 4.3. The Effects of Confusion and Catalog Reliability

We investigated the effects of confusion (Scheuer 1957; Condon 1974) and noise by generating Monte-Carlo simulations of our field and then using the technique used for the real image (§4.1) to find the sources. The simulations are based on the 14<sup>h</sup> source counts. We have assumed that, at high flux densities, the integral source counts have the form  $N(> S) = N_0 S^{-\alpha}$ , with  $N_0$  and  $\alpha$  chosen to match the 14<sup>h</sup> counts; while at flux densities below a transition flux density,  $S_t$ , we have assumed that the source counts have the form  $N(> S) = N_1 \ln(S)$ , with  $N_1$  chosen so that the source counts at low and high flux densities are the same at  $S = S_t$ , and  $S_t$  chosen so that the total flux density from all the sources equals the cosmic background radiation at 850 $\mu$ m (Fixsen et al. 1998). As the first stage in the Monte-Carlo experiment, we used these source counts to generate five representations of the 14<sup>h</sup> field with no noise component; for these fields, errors in the recovered fluxes and positions will be entirely the effect of source confusion. As the second stage, we generated five noise images, as in §4.1, and then used the assumed source counts to add sources to these images; for these fields, errors in the recovered fluxes and positions will be the effect of both confusion and noise.

Figure 4 shows the results. The top row of plots in this montage are for the fields with no noise and the bottom row are for the fields containing noise. The bottom row of plots is most relevant for considering the present reliability of the catalog, although a comparison of the two rows shows that it is a combination of noise and confusion which produces the effects we consider below. The bottom lefthand plot shows the flux of the source put in the simulation (the input flux,  $S_{in}$ ) plotted against the flux recovered by the source-finding technique (output flux,  $S_{out}$ ). This plot shows that our sample is surprisingly complete. A sample with  $S_{out} > 3$  mJy contains 90% of the sources with input fluxes brighter than this. However, the less gratifying result is that the fluxes of the sources in a sample will tend to be biased upwards; although the effect of confusion and noise can either increase or decrease the flux of a source, a flux-limited sample will preferentially contain sources whose flux densities have been boosted. The sizes of boost factors ( $S_{out}/S_{in}$ ) can be seen most easily in the bottom righthand plot, where this is plotted against the difference between input and output position. The median boost factor is 1.44 with a large scatter about this value.

Apart from biasing the fluxes of individual sources, this effect will produce a bias in the source counts, which has cosmological implications (§6.1). A comparison of the source counts produced from our recovered sources with the input source counts shows that the slope of the counts is unaffected but that the integral counts are shifted in flux by the average boosting factor. The correct source counts to use as the input to our simulation are the true source counts, whereas we necessarily had to use the measured source counts. Since the measured source counts will have been boosted from the true counts, our simulation will have overestimated somehwat the effect of confusion; thus the boosting factor we have deduced is strictly an upper limit.

The middle plot in the bottom row shows the difference between input and output positions plotted against output flux. Knowledge of the size of the positional errors is of course crucial for

any attempt to determine the optical/IR counterparts to the SCUBA sources. The plot shows that 19% of the SCUBA sources have positional differences greater than 6 arcsec. This means that if one searches for the optical/IR counterpart to a SCUBA source within a circle of radius 6 arcsec centered on the SCUBA source (we used five arcsec in Paper II), the true counterpart will lie outside this circle 19% of the time. This is strictly an upper limit for the reason discussed above. However, we also investigated this issue using a separate set of Monte-Carlo simulations, in which we placed artificial sources on our real image, and then tried to recover the sources using our standard algorithms. In these simulations, we found that 12% of the sources had positional differences greater than 6 arcsec. The combination of these two sets of simulations imply between 10 and 20% of the sources have positional differences greater than 6 arcsec.

Some insight into the nature of the sources with large positional discrepancies comes from the two righthand plots. A comparison of the two shows that there are almost three times as many sources with positional offsets greater than 6 arcsec when noise is added to the simulations as when there is only source confusion. The lower plot also shows that the median boost ( $\simeq 2.3$ ) for the sources with such large offsets is much greater than the average boost factor for the whole sample (1.44). This suggests that the sources with large offsets are produced by the proximity of one or more faint sources to noise peaks; thus the sources with large offsets and the  $\simeq 14\%$  of the sources expected to be spurious from Gaussian statistics (§4.1) are probably the same objects.

The results of these simulations are of course applicable to many of the other submillimetre surveys. Our survey contains about one source per forty beams, which is the traditional limit at which confusion begins to becomes important (Scheuer 1957; Condon 1974). Deeper surveys, such as that of the Hubble Deep Field (Hughes et al. 1998) are beyond this limit, which may explain why there has been so much disagreement about the optical/IR counterparts to the SCUBA sources in this field (Hughes et al. 1998; Richards 1999; Downes et al. 1999).

## 5. The Correlation With Other Surveys

### 5.1. ISO

The  $14^h$  field has been surveyed with ISO at  $6.75\ \mu\text{m}$  (Flores et al. 1999a) and at  $15\ \mu\text{m}$  (Flores et al. 1999b). We looked for objects that might be both SCUBA sources and ISO sources by looking for  $15\ \mu\text{m}$  sources that fall close to a SCUBA source. If an ISO source lies  $d$  arcsec from a SCUBA source, the probability of it not being related to the SCUBA source is  $1 - e^{-\pi n d^2}$ , in which  $n$  is the surface density of ISO sources. The low surface density of ISO sources means that it is possible to consider a much larger search radius than is possible when looking for optical counterparts (Paper II) and we chose a search radius of 10 arcsec. The simulations described in the last section show that the true positions of virtually all the SCUBA sources should lie within 10 arcsec of the measured position. The ISO positions, of course, have errors themselves ( $\simeq 3.7$  arcsec, Flores et al. 1999b), but these are rather less than the SCUBA errors, and in the many

cases where there is an optical counterpart (Flores et al. 1999b) we have used the position for this rather than the ISO position. Thus the SCUBA positional errors are the dominant source of error in this analysis, and since we are using a search radius that is large enough to allow for this, we should not have missed any genuine SCUBA-ISO association.

Table 4 lists the two ISO galaxies that fall within 10 arcsec of SCUBA positions and one ISO galaxy that is marginally outside this search radius. CUDSS 14.13 and 14.18 are almost certainly associated with ISO sources (ISO 0 and 5); the probability of a chance coincidence is small and the two ISO sources are the brightest  $15\mu\text{m}$  sources in Flores et al.’s list (see §6.3 for why this is a supporting argument). The positional difference between CUDSS 14.13 and the galaxy associated with ISO 0 is quite large (5.9 arcsec) but the SCUBA source is confused with another (§4.2) and thus the positional accuracy may be worse than usual. This field is quite interesting because there is a cluster of five ISO sources apparent on the image of Flores et al., and the coincidence of this cluster with the two confused SCUBA sources suggests that we may have found a cluster of dusty galaxies at a redshift of 1.15, the redshift of the galaxy associated with ISO 0. The third association is more speculative; the probability of the association being incorrect is only 8%, but given the size of our sample of SCUBA sources we would expect to find at least one unrelated ISO source falling this close to one of the SCUBA sources. We have only listed this association as a possibility because the SCUBA position is known to be inaccurate (§4.2), and henceforth we assume that the association is not genuine.

Only two of the 19 SCUBA sources are ISO  $15\mu\text{m}$  sources, and of the  $\simeq 50$   $15\mu\text{m}$  sources in this field only two are submillimetre sources. This confirms earlier claims that the ISO and SCUBA surveys are finding different sets of objects (Hughes et al. 1998; Lilly et al. 1999).

## 5.2. Radio

The  $14^h$  field has been surveyed with the VLA at 5 GHz and slightly less deeply at 1.5 GHz (Fomalont et al. 1991). We looked for associations between SCUBA sources and radio sources detected at  $>3\sigma$  on the original 5GHz radio image (kindly supplied by Dr. E. Fomalont). Because of the higher surface density of radio sources relative to the ISO sources (§5.1), it proved necessary to restrict the search radius to six arcsec to avoid too many false associations; this then creates the opposite problem that  $\simeq 10\text{--}20\%$  of the genuine associations will be missed (§4.3). The results are given in Table 5. Of the 19 SCUBA sources in our catalog, 16 fall in the useable area of the 5GHz radio image, and of these there are five which have radio sources within 6 arcsec. One of the SCUBA sources, 14.13, has two radio sources at about the same distance. We have assumed that the brighter radio source is the genuine association, because it is coincident with the galaxy associated with ISO 0 (§5.1). For the SCUBA sources which lie outside the useable area of the 5GHz map, we obtained upper flux limits from the 1.5GHz map, which we re-reduced.

The percentage of the SCUBA sources which are detected at radio wavelengths is 31% if only

the sources for which we have 5GHz data are considered and 26% if all the sources are included. Both percentages are much lower than the percentage of 71% detected at radio wavelengths by Barger, Cowie and Richards (2000) for a different SCUBA sample. We discuss the reasons for this difference in §6.2.

## 6. The Immediate Implications of the Survey

### 6.1. How much of the submillimetre background has been resolved?

The fraction of the 850 $\mu$ m background radiation that can be accounted for by simply replicating the sources found in the SCUBA survey over the sky is of great importance, because if this fraction is high (and if the SCUBA galaxies are also representative of the stronger submillimetre background at shorter wavelengths—§1), then they are responsible for a significant fraction of the total energy output of the galaxy population. To estimate this fraction, however, it is necessary to allow for the possibility of flux boosting (§4.3).

Fig. 3 shows the source counts. We have assumed that the *differential* counts have the power-law form,  $dN(< S)/dS = N_0 S^{-\alpha}$ , and determined  $\alpha$  using the standard Maximum Likelihood technique (Jauncey 1967), obtaining the value  $3.25 \pm 0.7$ ; the Monte-Carlo simulations (§4.3) show that this is relatively unaffected by the effects of confusion and noise. This value is consistent with the values of 3.2 (95% confidence limits of 2.6 and 3.9) estimated by Barger et al. (1999) and  $2.8 \pm 0.7$  estimated from the cluster survey (Blain et al. 1999b).

Using this value of  $\alpha$  and an estimate of  $N_0$  from the 14<sup>h</sup> counts, and making no correction for flux boosting, we estimate that 27% of the background at 850 $\mu$ m (Fixsen et al. 1998) is produced by individual sources brighter than 3 mJy. After a correction of 1.44 is made in flux to allow for flux boosting (§4.3), 19% of the background is produced by sources with true flux densities brighter than 2 mJy (the steepness of the source counts means that the fraction of the background produced by sources with true flux densities brighter than 3 mJy falls to 8%). The deepest blind survey is of the Hubble Deep Field (Hughes et al. 1998), which had a sensitivity limit of 2 mJy and which resolved about 30% of the background into individual sources (this is not significantly higher than our value because the HDF counts were rather lower than ours—Fig. 3). Flux boosting should be at least as bad in the HDF, and if the same correction is made, 21% of the background is produced by sources with true flux densities brighter than 1.4 mJy. There is some information about the source counts fainter than 2 mJy (Fig. 3), but this information consists of a fluctuation analysis in the HDF and three sources in the cluster lens survey with unlensed flux densities less than 3 mJy (Blain et al. 1999b; Blain et al. 1999c). Therefore, a conservative conclusion would be that 20% of the background at 850 $\mu$ m has been resolved into individual sources.

## 6.2. The radio-submillimetre relation: structures and redshift distributions

Radio observations of SCUBA survey fields are important for three reasons: to provide more accurate positions; to determine whether AGN or young stars are heating the dust; to provide redshift estimates. The physical basis of the usefulness of radio observations is that at low redshift the far-infrared and radio emission from star-forming galaxies are tightly correlated (Helou, Soifer & Rowan-Robinson 1986; Devereux and Eales 1989), presumably because the dust is being heated by high-mass stars, which then rapidly form supernovae, generating the relativistic electrons necessary for radio emission. Not only are the dust emission and radio emission correlated globally but they are also correlated spatially (Eales et al. 1988) and thus high-resolution radio observations are a way of inferring whether the dust emission is extended, as would be expected for star-forming galaxies, or unresolved, as would be the case for AGN. The shape of the radio-submillimetre spectral energy distribution for a typical star-forming galaxy means that, in the absence of evolution, the radio to  $850\mu\text{m}$  flux ratio will depend strongly on redshift, and Carilli & Yun (1999) have suggested that this ratio might be a good redshift indicator.

The most basic things the radio observations provide are more accurate positions for individual sources and information about the overall accuracy of the SCUBA positions. Of the five SCUBA-radio associations, the median difference between the radio and submillimetre positions is 2.0 arcsec (Table 5). This may be compared with the predictions of the Monte-Carlo simulations (§4.3) shown in the bottom middle panel of Fig. 4. Discarding the Monte-Carlo sources with positional errors greater than 6 arcsec, since the radio-SCUBA associations would have been missed completely (§5.2), the predicted median error is 3.5 arcsec. Although the number of sources is small, the fact that the median observed difference is rather smaller than the median predicted difference suggests that the Monte-Carlo simulations did give a conservative estimate of the positional errors.

Of the five radio sources, four have angular sizes of  $\simeq 1\text{-}2$  arcsec (Fomalont et al. 1991). Sources this size would only have barely been resolved by the VLA beam but, if correct, this result is interesting for two reasons. First, it suggests that these are not AGN but star-forming galaxies. Second, the implied physical sizes ( $10h_{50}^{-1}$  kpc for  $z > 1$ ) are much larger than the sizes of the starburst regions in nearby ULIRG's (Eales et al. 1988), and so this may be the first indication that the SCUBA sources are objects in which galaxy-wide starbursts are occurring, rather than the nuclear starbursts seen in low-redshift ULIRG's.

Carilli & Yun (1999) used models to investigate how the ratio of submillimetre to radio flux should depend on redshift for star-forming galaxies. Dunne, Clements and Eales (2000) have recently used the radio, submillimetre, and far-infrared data for the 104 galaxies in SLUGS (§1) to estimate how this ratio should depend on redshift for real star-forming galaxies, and in particular how the dispersion in this ratio should depend on redshift, since this is crucial for determining the accuracy of redshift estimates made with this technique. Fig. 5 shows their estimate of how this ratio should depend on redshift, and of the  $\pm 1\sigma$  uncertainty in using this ratio to estimate redshifts. Also plotted in the figure are the submillimetre to radio ratios for all the galaxies detected

in SCUBA surveys which have spectroscopic redshifts and useful radio data. Of the six galaxies plotted, five are in excellent agreement with the predictions, which is additional evidence that the SCUBA galaxies are mostly star-forming galaxies rather than AGN.

We have used these curves to estimate redshifts and redshift limits for our sample. The curves are calibrated using 1.4-GHz fluxes, and we have converted our 5-GHz fluxes to this frequency using the spectral indices listed in Fomalont et al. (1991). For the SCUBA sources with only radio upper limits we have converted the 5GHz upper limits to 1.4GHz upper limits using a radio spectral index of 0.7, typical of the sources found in deep 1.4GHz surveys (Richards 2000). We have used these upper flux limits and the median curve in Fig. 5 to estimate lower redshift limits for these sources. The redshift estimates and limits are given in Table 5.

We have also used Fig. 5 to estimate redshifts for two other samples: (i) the cluster lens survey (Smail et al. 2000); (ii) the sample of sources with  $S_{850\mu\text{m}} > 6\text{mJy}$  from the Hubble Flanking Fields (HFF; Barger, Cowie and Richards 2000). Fig. 6 shows the redshift distributions for the three samples. Much of the information in all the distributions consists of limits rather than measurements, and so we have investigated the statistics of these distributions using the ASURV Rev 1.2 package (La Valley et al. 1992), which implements the techniques for treating censored data described in Feigelson & Nelson (1985). The results are given in Table 6. The median redshift for the  $14^h$  sources is 2.05. Although the large number of limits for this sample mean that this estimate is highly uncertain (shown by the ASURV package’s failure to produce 95% error limits for this sample—Table 6), it is close to the estimated median redshift of the optical counterparts of the first 12 sources in our SCUBA survey (Paper II). The median redshifts for all the samples lie in the range 1.5 to 2.5, with the means lying in the range 1.9 to 2.7. We compared the distributions for the individual samples using the Peto-Prentice generalised Wilcoxon test, finding that the differences between them are not significant. If all the samples are combined together, the median redshift is 2.4, with 95% confidence that it lies between 1.9 and 3.5.

Finally, we consider the reason for the different radio detection rates for our sample and that of the HFF sources. Barger et al. detected five out of seven SCUBA sources, giving a detection rate of 71% compared with 31% for the  $14^h$  sources (§5.2). The radio observations were of similar sensitivity, but the  $850\mu\text{m}$  flux limit of Barger et al. was significantly brighter than our limit; thus, at a given redshift, Barger et al. would have been able to detect sources with a higher ratio of submillimetre to radio flux. This must be part of the explanation but part of it may also be the small numbers of sources involved. Although there is no significant difference between any of the samples, the median redshift of the HFF sources is the lowest of the three samples (Table 6); and since the lower the redshift, the lower the predicted submillimetre to radio flux ratio, the high radio detection rate for the HFF sources may partly be a statistical fluctuation.

### 6.3. The spectral energy distributions of high-redshift dusty galaxies

We investigated the significance of the  $15\mu\text{m}/850\mu\text{m}$  and  $450\mu\text{m}/850\mu\text{m}$  flux ratios of the galaxies found in the SCUBA and ISO surveys by comparing the measured ratios and limits with the predictions for three standard spectral energy distributions (SED). The first two are taken from Schmitt et al. (1997), who list average spectral energy distributions (SED) for a number of types of galaxy. We have used the SEDs for spirals and for high-extinction starbursts (SBH). Since Schmitt et al. did not have access to many submillimetre data when compiling these SEDs, we have created new SEDs at wavelengths greater than  $60\mu\text{m}$ , matching these on to the listed SEDs at this wavelength. For the spiral galaxy, we used the two-component fit to the far-infrared and submillimetre data for NGC 891 of Alton et al. (1998). For the starburst, we assumed a dust temperature of 48K and a dust-emissivity index of 1.3, a good fit to the data for the archetypical starburst M82 (Hughes, Gear and Robson 1994). As the SEDs in Schmitt et al. are based on observations of galaxies that appear in the IUE archive, even their high-extinction starbursts are likely to have much less dust extinction than the ULIRGs revealed by IRAS. Therefore, as a third standard SED, we used the SED of the archetypical ULIRG, Arp 220. At wavelengths greater than  $60\mu\text{m}$ , we assumed a dust temperature of 42.2K and a dust emissivity index of 1.2, which is a good fit to the submillimetre and far-infrared fluxes (Dunne et al. 2000). We extended this SED to shorter wavelengths by interpolating between the flux densities of Arp 220 measured by IRAS and with ground-based telescopes (Carico et al. 1988).

Fig. 7 shows the  $15\mu\text{m}/850\mu\text{m}$  flux ratios and limits for the ISO and SCUBA galaxies plotted against their redshift, together with the predictions of the three SEDs. The ISO galaxies are the ones with spectroscopic redshifts in Catalogue 1 of Flores et al. (1999b), and for simplicity the lower limits on the flux ratio have been calculated assuming an upper limit to the  $850\mu\text{m}$  flux density of 4 mJy. The upper limits to the flux ratio for the SCUBA galaxies have similarly been calculated using an upper limit to the  $15\mu\text{m}$  flux of 0.18 mJy. Only two of the SCUBA galaxies have spectroscopic redshifts, and for the remainder we have used the redshift estimates or limits obtained from the radio method (§6.2).

There are a number of straightforward conclusions that one can reach from this diagram. The flux ratios of the ISO galaxies are consistent with the predictions of the spiral and SBH SEDs but are not consistent in most cases with the prediction of the Arp 220 SED. The explanation for this is quite simple. Arp 220 has a very steep SED between the near-infrared and  $60\mu\text{m}$ , presumably because the extinction in this object is so high that even the long-wavelength emission is significantly absorbed. Therefore, its  $15\mu\text{m}$  flux falls rapidly with redshift. Thus the ISO mid-infrared surveys are picking up galaxies in which the extinction is much more modest than in the ULIRGs discovered with IRAS. Note, this shows the care needed in modelling the results of the mid-infrared surveys; it is not simply a matter of extrapolating models based on IRAS results (see Roche and Eales 1999 for further discussion). A consideration of the curves also shows why it is the two ISO galaxies with the highest  $15\mu\text{m}$  flux densities which are associated with SCUBA sources (§5.1). Given the high flux ratios predicted by the spiral and SBH models at  $z < 1$ , only a galaxy with a very high

$15\mu\text{m}$  flux would also be detected at  $850\mu\text{m}$ .

In contrast to the ISO galaxies, the limits for the SCUBA sources are consistent with the Arp 220 SED, are always inconsistent with the spiral SED, and generally disfavour the SBH SED. These results show that the mid-infrared and submillimetre surveys are picking up different classes of galaxy.

Fig. 8 shows the ratio of  $450\mu\text{m}$  to  $850\mu\text{m}$  flux for the sources in this paper and those in Paper I and II which have redshift measurements, estimates, or limits. Apart from the predicted curves based on the SEDs discussed above, the plot also shows a predicted curve based on the SED of the high-redshift galaxy IRAS 10214+4724, which has an estimated dust temperature of 80K and a dust emissivity index of 2 (Downes et al. 1992). The first conclusion one can draw is that whereas the SEDs of the SCUBA galaxies are always consistent with the first three models, they are sometimes inconsistent with an SED of this kind (a single temperature and a dust emissivity index of 2), something which is also true of the galaxies in SLUGS (Dunne et al. 2000). The predictions for all the SEDs initially remain constant with redshift, because at low redshift both the  $450\mu\text{m}$  and  $850\mu\text{m}$  observations are sampling the Rayleigh-Jeans tail of the SEDs; it is only when, in the rest-frame of the galaxy, the  $450\mu\text{m}$  observations are getting close to the peak of the SED that the predictions begin to fall. This occurs at a lower redshift for a lower dust temperature, which explains why the prediction for the spiral SED, which includes emission from 15K dust, starts to fall at a lower redshift than the other two. The  $3\sigma$  limit on the average  $450\mu\text{m}/850\mu\text{m}$  flux ratio for the SCUBA galaxies (§4.1) is shown by the horizontal line. If these galaxies are typically at redshifts of  $\sim 2$ , as suggested by the radio method (§6.2), then this limit implies the dust in the SCUBA galaxies is colder than that found in Arp 220 and M82. The alternative is that the galaxies are generally at much higher redshifts than indicated by the radio method. The first possibility seems most likely because there is no reason to doubt the radio method and is of great interest because it is the second piece of evidence (the radio sizes being the other) that SCUBA galaxies are not simply high-redshift ULIRGs.

## 7. The Cosmological Significance of the SCUBA Sources

This section describes modelling of the SCUBA population with the aim of answering some of the key questions about this population (§1): (1) Are the high-redshift galaxies discovered at optical wavelengths through the Lyman break technique a completely separate population from the SCUBA galaxies? (2) Did the universe have a Dark Age in which 10 times as much star formation was hidden by dust as appears at optical wavelengths? (3) Does the submillimetre luminosity density keep on increasing with redshift or does it decrease above  $z \sim 2$ ? (4) If the SCUBA galaxies are proto-ellipticals, when exactly did ellipticals form? About a fifth question, whether the dust is heated by AGN or young stars, we can say little beyond noting that both the radio structures and the radio-to-submillimetre flux ratios (§6.2), as well as the first deep X-ray surveys (Fabian et al. 2000; Hornschemeier et al. 2000), suggest that it is the latter; and this is what will be assumed

through the rest of this section. The focus of the modelling described in §7.2 will be on determining why there are conflicting answers to many of these questions. First, however, we will consider separately the first question.

### 7.1. Are the Lyman-Break and SCUBA Galaxies the same Population?

As Lyman-break galaxies are found from their properties in the rest-frame ultraviolet and SCUBA galaxies are found from their dust emission, one might expect that the statistical properties of the two populations should be very different. Adelberger and Steidel (2000), however, have recently suggested that the two populations are essentially the same, and that there is no evidence that a significant fraction of the star-formation in the universe occurred in galaxies so heavily obscured that they could not be detected in UV-selected surveys. One test of this idea is to determine directly the submillimetre properties of the Lyman-break galaxies. Although SCUBA observations of individual Lyman-break galaxies have resulted in only a single detection (Chapman et al. 2000), Peacock et al. (2000) have claimed a statistical detection of the population by summing the submillimetre emission at the positions of Lyman-break galaxies in the deep SCUBA image of the Hubble Deep Field. The greatest uncertainty in this claim is the fact that Lyman-break galaxies are highly-biased and thus highly-clustered systems (Steidel et al. 1998; see Fig. 4 of Peacock et al.) and if SCUBA galaxies are similarly highly-biased highly-clustered systems following the same large-scale structure as the Lyman-break galaxies, the small number of SCUBA beams in the Hubble Deep Field means that the technique of Peacock et al. might yield a detection even if the Lyman-break galaxies themselves contain no dust. Nevertheless, in this section we assume the claim is correct and investigate its implications by predicting the contribution of Lyman-break galaxies to the submillimetre background and source counts.

Adelberger and Steidel predicted the global submillimetre properties of the Lyman-break galaxies by using correlations between bolometric luminosity and fluxes at UV, mid-infrared and submillimetre wavelengths established for local starbursts. Here we adopt the simpler approach of using the average ratio of submillimetre to optical flux measured for the Lyman-break population by Peacock et al. (2000). We predicted the  $850\mu\text{m}$  source counts and the submillimetre background from the Lyman-break population in the redshift range  $1 < z < 5$ . We used the average ratio of  $850\mu\text{m}$  to optical flux for the 20 Lyman-break galaxies in Table 1 of Peacock et al. and the I-band luminosity function given by Steidel et al. (1999) for Lyman-break galaxies at  $z \sim 3$ ; we assumed that there is no cosmic evolution in the luminosity function over this redshift range. We have also implicitly assumed that the submillimetre to optical flux ratio found by Peacock et al. for the most luminous Lyman-break systems applies to the whole population. Even if the Lyman-break population has been detected in the submillimetre, there is no information about their dust temperatures; so we tried two dust temperatures, 20K and 40K, and assumed a value for the dust emissivity of 1.2, similar to that seen for the low-redshift galaxies M82 and Arp 220 and consistent with the limited amount of multi-wavelength submillimetre photometry for SCUBA galaxies (§6.3). Fig. 9

shows the predicted submillimetre background and source counts.

The predicted contribution of the Lyman-break galaxies to the background depends critically on dust temperarure: if the dust temperature is 40K, the Lyman-break galaxies produce most of the submillimetre background; if the dust temperature is 20K, their contribution to the overall background is not so important, although they do produce the entire background at long wavelengths. The predicted source counts do not match the observed source counts at high flux densities although the discrepancy is only a factor of 5.3 in flux density (or 3.8 if flux-boosting is taken into account).

Thus this simple model shows that, if Peacock et al. are correct, the Lyman-break population might be an important component of the submillimere source counts and background. However, there are two important points to consider. First, if the submillimetre to optical flux ratio derived for the Lyman-break galaxies applied only to the most luminous systems, then since the background is dominated by low-luminosity systems, this conclusion would be incorrect. Second, at  $z < 3$ , the  $850\mu\text{m}$  emission is approximately proportional to  $M_d T_d$ , in which  $M_d$  is dust mass and  $T_d$  is dust temperature. Thus, dust mass is as important a predictor of  $850\mu\text{m}$  flux density as dust temperature; and if the Lyman-break galaxies were massive galaxies, it would not be surprising for the most luminous Lyman-break galaxies to be detected by SCUBA at a flux level a few times less than the sources revealed in the blind surveys. There is at present little evidence as to the masses of the Lyman-break galaxies, although measurements of nebular lines in the infrared for a handful of objects suggest that, in general, Lyman-break galaxies are not very massive galaxies (Pettini et al. 1998).

Finally, we note (as we did in §1) that the optical properties of the SCUBA sources do not in general support this hypothesis. If it were correct, the optical/IR counterparts to the SCUBA sources should be bright enough to be detected in the Lyman-break surveys; and this should be especially true of the counterparts to the brighter SCUBA sources. Consider, however, the brightest  $14^h$  source, CUDSS 14.1 (Gear et al. 2000). We have estimated, using the radio technique (§6.2), that its redshift is  $\simeq 2$ . From its measured magnitudes (Gear et al. 2000), we estimate that if this source were moved out to a redshift of 3, the redshift of the Lyman-break galaxies, its magnitude would be  $I_{\text{AB}} \simeq 27$ . This is two magnitudes fainter than the limit of the Lyman-break surveys.

There are a large number of uncertainties in the discussion above. However, we conclude, mainly because of the argument in the last paragraph, that the SCUBA galaxies and the Lyman-break galaxies are largely separate populations. We suspect that the submillimetre detections that are beginning to be made of the Lyman-break galaxies are largely caused by the sensitivity of the  $850\mu\text{m}$  emission to dust mass; if some of the Lyman-break galaxies are massive galaxies, one would expect detections at roughly the level found.

## 7.2. The Hidden Star-Formation History of the Universe

We addressed the remaining questions by investigating how the submillimetre properties of galaxies must change with redshift in order to reproduce the observations: the submillimetre background, the source counts, and the redshift distribution. The simplest types of cosmic evolution are luminosity evolution, in which the luminosities of individual galaxies change with time but the total number of galaxies remain the same, or density evolution, in which the luminosities stay the same but the total number changes. In the submillimetre waveband, however, density evolution does not work, because the strength of evolution needed to reproduce the  $850\mu\text{m}$  source counts leads to much too high a submillimetre background (Paper I; Blain et al. 1999a). We therefore assumed that the bolometric luminosities of the dust in all galaxies vary with redshift in the following way:

$$L_{bol} = L_0(1+z)^p \text{ at } z < z_t, \quad (1a)$$

and

$$L_{bol} = L_0(1+z)^q \text{ at } z > z_t, \quad (1b)$$

in which  $z_t$  is a transition redshift. Our method was to try thousands of combinations of  $p$ ,  $q$ ,  $z_t$  in different cosmologies in order to find ranges of these values consistent with the observations. Since there are many combinations of these parameters that do give acceptable fits to the data, there is no need to try a more complicated model—and this method does give valuable insight into why there is so much disagreement about the cosmological significance of the SCUBA galaxies.

The local submillimetre luminosity function which formed the basis of the models was the  $850\mu\text{m}$  luminosity function derived, as part of the SCUBA Local Universe and Galaxy Survey (Dunne et al. 2000), from SCUBA observations of 104 galaxies from the IRAS Bright Galaxy Survey (BGS; Soifer et al. 1989). In making predictions of the  $850\mu\text{m}$  source counts and redshift distribution, rather than working from the local luminosity function, we started from the derived spectral energy distributions of the 104 galaxies and used standard accessible volume techniques (Avni & Bahcall 1980). To give a specific example, the number of galaxies with  $S_{850\mu\text{m}} > 4 \text{ mJy}$  in an area of sky  $A_{SCUBA}$  is given by

$$N(> 4\text{mJy}) = \sum_i \frac{A_{SCUBA} \int_0^{z(P_i, S_{850\mu\text{m}} = 4\text{mJy})} dV}{A_{BGS} \int_0^{z(P_i, S_{60\mu\text{m}} = 5.24\text{Jy})} dV}$$

in which  $A_{BGS}$  is the solid angle of the original sample from which the galaxy was drawn, the sum is over all 104 galaxies, and  $V$  is comoving volume. The upper redshift limits are the redshifts to which the  $i$ 'th galaxy would have been seen in the BGS and in a sample with  $S_{850\mu\text{m}} > 4\text{mJy}$ . These were calculated using the single-temperature spectral energy distribution (SED) for each galaxy found by Dunne et al. to be a good fit to the far-infrared and submillimetre flux densities

(this does not imply that there is dust of only one temperature in the galaxy, merely that this is an adequate representation of the empirical SED). In the first set of models, to implement the cosmic evolution, we assumed that the amplitude of the SED of each galaxy, but not its spectral shape, evolves with redshift according to equation (1).

We used a slightly more complicated approach to predict the submillimetre background because there is a significant contribution to the background from galaxies with lower luminosities than are properly sampled by the  $850\mu\text{m}$  local luminosity function of Dunne et al. Therefore, we used the  $60\mu\text{m}$  local luminosity function (Saunders et al. 1990) as our basic local luminosity function, using the submillimetre data from SLUGS to extrapolate this into the submillimetre waveband. The dust temperature of the SLUGS galaxies is correlated with  $60\mu\text{m}$  luminosity, with the form

$$T_d = 4.61 \times \log_{10} L_{60} - 72.7$$

in which  $L_{60}$  is monochromatic luminosity at  $60\mu\text{m}$  in Watts  $\text{Hz}^{-1} \text{ sr}^{-1}$ . We used this equation and the median dust emissivity index for the galaxies in the SLUGS (1.2, Dunne et al. 2000) to derive a far-infrared to submillimetre SED at each  $60\mu\text{m}$  luminosity. As for the source counts, we implemented cosmic evolution by assuming that the SED did not change its shape with redshift, merely its amplitude.

We tried to reproduce only three sets of observations: the overall submillimetre background, the  $850\mu\text{m}$  source counts, and the redshift distribution of the SCUBA galaxies. In a subsequent paper we will extend the models to consider the ISO results and also to make predictions for SIRTF and SOFIA (Eales and Dunne, in preparation). In attempting to reproduce the  $850\mu\text{m}$  counts, we corrected the observed counts for the effect of flux-boosting (§4.3); thus the observed counts at 4 mJy are assumed to represent the real counts at 2.8 mJy. A model was judged to provide an acceptable fit to the observations if it satisfied the following criteria: (i) the predicted submillimetre background was at no wavelength more than a factor of two different from the observed background; (ii) the predicted  $850\mu\text{m}$  source counts at 2.8 mJy were no more than  $2\sigma$  different from the observed counts at 4 mJy; (iii) the fraction of galaxies predicted to be at redshifts less than two in a sample with  $S_{850\mu\text{m}}(\text{observed}) > 4.0\text{mJy}$  lay between 0.2 and 0.8. These criteria of acceptability are quite generous and recognise that much of the uncertainty in the submillimetre waveband is systematic rather than statistical; the main uncertainty in the background, for example, is whether the subtracted foregrounds have been adequately modelled rather than signal-to-noise. The redshift criterion is our admittedly subjective estimate of how uncertain this fraction is (§6.2).

Fig. 10 shows the predictions of the models for a universe with  $\Omega_0 = 1$  and no galaxies or equivalently no dust beyond a redshift of 5. Each plot, which is for a separate value of  $z_t$ , shows the low-redshift exponent for the evolution model,  $p$ , plotted against the high-redshift exponent,  $q$ . The greyscale shows the fraction of galaxies predicted to lie at  $z < 2$  in our canonical SCUBA sample with  $S_{850\mu\text{m}}(\text{observed}) > 4.0 \text{ mJy}$ . The continuous line encloses models which give acceptable predictions for all the data; the dashed line shows the additional region in which the models match

the source counts and the background but do not predict the right fraction of sources at  $z < 2$ . For  $z_t = 1, 1.5, 2$  there are many acceptable models, with strong evolution below the transition redshift and with either negative, or, at the most, mild positive evolution above this redshift. For  $z_t = 2.5$ , the only models which fit the data are ones with strong negative evolution beyond the transition redshift.

We also used the models to make predictions for a universe with  $\Omega_0 = 0.2$ ,  $\Lambda/(3H_0^2) = 0.8$ . There are no models that fit both the  $850\mu\text{m}$  source counts and submillimetre background for this cosmology, for the following reason. The SCUBA sources are high-luminosity sources whereas there is a significant contribution to the background from low-luminosity sources. In this cosmology, models which generate enough high-luminosity sources to reproduce the source counts, generate so many low-luminosity sources that the predicted background is too high. We could produce acceptable models by only including evolution for sources above some critical luminosity, but this is beyond the scope of this paper.

In all of these models we assumed that the spectral shape of the SED of each SLUGS galaxy is independent of redshift and implemented the required bolometric luminosity evolution by having the normalization of this SED change with redshift. It is possible, however, that the temperature of the dust in galaxies also changes with redshift. In accord with our approach of exploring the full range of models that might give acceptable agreement with the observations, we tried the following model. In this variation on the basic model, the SEDs of the SLUGS galaxies remain constant until the transition redshift, where the temperature of the dust is then increased by a factor of 1.5, with the normalization of the SED scaled appropriately so that there is not a sudden jump in bolometric luminosity. This abrupt change in the dust temperature is undoubtedly unphysical but is the simplest way of investigating the possibility that the average dust temperature at high redshift is much greater than it is today. In the model the typical dust temperatures of the SLUGS galaxies above the transition redshift are 45–65K, not inconsistent with the limited multi-wavelength submillimetre photometry of SCUBA sources (§6.3) and much lower than the dust temperature of 80K measured for the high-redshift galaxy IRAS 10214+4724 (Downes et al. 1992). Figs 11 and 12 show the results for this model for maximum redshifts of 5 and 10. Both figures show that there are now acceptable models in which the bolometric luminosity keeps on rising with redshift above the transition redshift. The reason for this can be seen by considering the SED of a galaxy at  $z \sim 3$ . Increasing the dust temperature of such a galaxy increases its bolometric luminosity by a large factor but has a much smaller effect on its  $850\mu\text{m}$  flux density which, even at this redshift, is emitted from the galaxy on the Rayleigh-Jeans tail of the SED. Thus the  $850\mu\text{m}$  source counts do not provide a strong constraint on this model. The increase in the bolometric luminosity has, of course, a large effect on the predicted background; but the increase in temperature means that the increase in the background occurs at wavelengths of  $\sim 200\mu\text{m}$ , where the observed background is at a maximum.

Now consider the questions raised at the start of this section, starting with whether the submillimetre luminosity density has a maximum. Figs 10–12 show that there are acceptable models in

which the submillimetre luminosity density reaches a maximum and also ones in which it increases monotonically with redshift. Thus the observations at present are insufficient to decide between these two possibilities.

Now consider the fraction of the star formation that is hidden by dust at low and high redshift. Fig. 13 shows bolometric dust luminosity plotted against redshift for all acceptable models. We will assume that this represents the energy emitted by young stars that is absorbed by dust. It is also necessary, of course, to estimate the optical/UV luminosity density associated with the young stars that is not absorbed by dust. The main uncertainty in doing this is that a large part of the optical light from galaxies is not from young stars but from evolved stars. We made the simple assumption that all the light from galaxies at wavelengths less than 5000Å is from young stars. We then estimated the optical/UV luminosity density in the local universe using the galaxy luminosity functions for galaxies of different morphological types given by Folkes et al. (1999) and the SEDs for galaxies of different morphological types given by Coleman, Wu and Weedman (1980). At high redshift, we started with the luminosity function given by Steidel et al. (1999) for Lyman break galaxies at  $z \sim 3$ . This luminosity function is at a rest-frame wavelength of  $\sim 2000\text{\AA}$ , and it is necessary to make some assumption about the typical SED of a Lyman-break galaxy in the wavelength range  $2000\text{\AA} < \lambda < 5000\text{\AA}$ , about which little is known. In practice, we made two estimates of the luminosity density, one assuming that the flux density per Hertz of a Lyman break galaxy is flat in this wavelength range and one using the SED given for west MMD11 by Adelberger and Steidel (2000). These estimates differed by 30% and we took the average of the two.

These estimates are shown in Fig. 13. At low redshift the percentage of the light from young stars that is hidden by dust is about 50%. At high redshifts, there are models in which this percentage is less but also models in which 90% of the light from young stars is absorbed by dust. Thus conclusions that the universe had a ‘Dark Age’ in which 90% of the light is absorbed by dust (Hughes et al. 1998; Barger, Cowie & Richards 2000) are premature, but neither can one rule out this possibility.

Finally there is the question of the origin of ellipticals. The colours and spectra of nearby ellipticals have traditionally been used to argue that most of the stars in ellipticals form at a high redshift (e.g. Bower, Lucey & Ellis 1992). If most of the stars in ellipticals formed at, for example,  $z > 3$ , then given the quantity of metals associated with nearby ellipticals (Edmunds and Phillipps 1997), about half the stars that have ever formed should have formed beyond this redshift. For each model we have calculated the fraction of stars that have formed by a redshift  $z$  using the following formula:

$$f = \frac{\int_{t(z_{max})}^{t(z)} L_{bol}(t') dt'}{\int_{t=0}^{t(z_{max})} L_{bol}(t') dt'}.$$

This implicitly makes the assumption that the star-formation rate is proportional to the bolometric luminosity. Fig. 14 shows  $f$  for all acceptable models. If dust temperature does not change with

redshift, then the largest percentage of star formation that has occurred by a redshift of three is  $\simeq 15\%$ , similar to the conclusion of Paper II from the redshifts of the optical counterparts. If dust temperature does evolve, this percentage rises to 32%; and the percentage would also rise in the analysis of Paper II if the dust temperature were allowed to evolve in this way. Thus we can not rule out the possibility that a significant fraction of stars have formed by this redshift.

It is clear that there are two types of observation which would allow substantial progress to be made. First, measurements of the temperature of the dust in the SCUBA galaxies would make it possible to estimate directly the bolometric luminosity of individual sources and of the population as a whole, which are crucial for all the questions. This should be possible through short-wavelength observations with SCUBA and, in the future, through observations with SOFIA and SIRTF. Second, the predicted redshift distributions shown in Figs 10-12 show that determining redshifts of more SCUBA galaxies would immediately rule out many models. It will be possible to make progress here through deep radio observations and millimetre/submillimetre interferometry, to obtain more accurate positions, and through optical/IR imaging and spectroscopy on 8-10m telescopes.

## 8. Conclusions

We have used the SCUBA submillimetre camera to survey an area of  $\simeq 50$  arcmin $^2$ , detecting 19 sources down to a  $3\sigma$  sensitivity limit of between 3 and 4 mJy at 850 $\mu$ m and obtaining the following results:

1. Of the 19 sources, 16 fall in a region with radio observations with  $\mu$ Jy sensitivity, and of these five are detected at radio wavelengths. The radio/submillimetre flux ratios and radio sizes suggest that the dust in these galaxies is being heated by young stars rather than AGN, although the radio sizes also suggest that the stars are being formed over a much larger region than is seen for low-redshift Ultra-Luminous Infrared Galaxies (ULIRGs).
2. We have used the radio to submillimetre flux ratio to estimate that the median redshift of the SCUBA sources is  $\sim 2$ . The redshift distribution is consistent with that determined in other surveys.
3. By coadding the 450 $\mu$ m emission at the positions of the 850 $\mu$ m sources, we obtained a  $3\sigma$  upper limit to the average 450 $\mu$ m/850 $\mu$ m flux ratio of 1.9, which implies that either the dust in the SCUBA galaxies is generally colder than in ULIRGs or that they are generally at  $z \gg 2$ .
4. A comparison of the SCUBA image with the 15 $\mu$ m image of this field obtained with ISO shows that only two of the 19 SCUBA sources were detected at 15 $\mu$ m, and, conversely, only two of the 50 ISO sources were detected at 850 $\mu$ m. A comparison of the 15 $\mu$ m/850 $\mu$ m flux ratios with predictions based on model spectral energy distributions shows that this result is

not simply caused by the submillimetre and mid-infrared surveys being sensitive to different redshift ranges, but that the ISO surveys will tend to have missed ULIRGs.

5. Monte-Carlo simulations of the field show that the fluxes of sources in all SCUBA surveys will have been significantly biased upwards by the effects of source confusion and noise, leading to an overestimate of the fraction of the  $850\mu\text{m}$  background that has been resolved by SCUBA. We reach the conservative conclusion that  $\simeq 20\%$  of the background at  $850\mu\text{m}$  has been resolved by SCUBA. The simulations have also been used to quantify the effects of confusion on source positions.

We have used the SCUBA Local Universe and Galaxy Survey and simple evolution models to address the major questions about the SCUBA sources: (1) what fraction of the star formation at high redshift is hidden by dust? (2) Does the submillimetre luminosity density reach a maximum at some redshift? (3) If the SCUBA sources are proto-ellipticals, when exactly did ellipticals form? The observations are not yet good enough, however, to answer these questions: there are acceptable models in which, at high redshift, 10 times as much star formation is hidden by dust as is seen at optical wavelengths, but also ones in which the star formation hidden by dust is less than that seen optically; there are acceptable models in which the submillimetre luminosity density reaches a peak, but also ones in which it continues to rise with redshift; finally there are acceptable models in which very little star formation occurred before a redshift of three (as might be expected in models of hierarchical galaxy formation), but also ones in which 30% of the stars have formed by this redshift. The models show that the keys to answering these questions are measurements of the dust temperatures and redshifts of the SCUBA sources.

We are grateful to the many members of the staff of the Joint Astronomy Centre, in particular Wayne Holland, that have helped us with this project. We thank Dr. E. Fomalont for allowing us to use his deep VLA image. Research by Simon Lilly is supported by the Natural Sciences and Engineering Research Council of Canada and by the Canadian Institute of Advanced Research. Research by David Clements, Loretta Dunne, Stephen Eales, and Walter Gear is supported by the Particle Physics and Astronomy Research Council. The JCMT is operated by the Joint Astronomy Center on behalf of the UK Particle Physics and Astronomy Research Council, the Netherlands Organization for Scientific Research and the Canadian National Research Council.

## REFERENCES

Adelberger, K.L. & Steidel, C.C. 2000, ApJ, submitted (astro-ph 0001126).  
Alton, P.B., Bianchi, S., Rand, R.J., Xilouris, E.M., Davies, J.I. & Trewella, M. 1998, ApJ, 507, L125.

Archibald, E.N., Dunlop, J.S., Hughes, D.H., Rawlings, S., Eales, S. & Ivison, R. 2000, MNRAS, submitted (astro-ph 0002083).

Avni, Y. & Bahcall, J.N. 1980, ApJ, 235, 694.

Barger, A.J. et al. 1998, Nature, 394, 428.

Barger, A.J., Cowie, L.L. & Sanders, D.B. 1999, ApJ, 518, L5.

Barger, A.J., Cowie, L.L. & Richards, E.A. 2000, AJ, 119, 2092.

Bernstein, R.A. 1999, “The Low-Surface Brightness Universe”, IAU Col. 171, ASP Conference Series, Vol. 170, eds J.I. Davies, C. Impey and S. Phillipps, p341.

Blain, A.W., Smail, I., Ivison, R.J. & Kneib, J-P. 1999a, MNRAS, 302, 632.

Blain, A.W., Kneib, J.-P., Ivison, R.J. & Smail, I. 1999b, ApJ, 512, L87.

Blain, A.W., Ivison, R., Kneib, J.-P. & Smail, I. 1999c, “The Hy-Redshift Universe”, eds A.J. Bunker and W.J.M. van Breugel.

Bond, J.R., Carr, B.J. & Hogan, C.J. 1986, ApJ, 306, 428.

Bond, J.R., Carr, B.J. & Hogan, C.J. 1991, ApJ, 367, 420.

Bower, R.G., Lucey, J.R. & Ellis, R.S. 1992, MNRAS, 254, 601.

Carico, D.P., Sanders, D.B., Soifer, B.T., Elias, J.H., Matthews, K. & Neugebauer, G. 1988, AJ, 95, 356.

Carilli, C.L. & Yun, M.S. 1999, ApJ, 513, L13.

Chapman, S.C. et al. 2000, MNRAS, submitted.

Coleman, G.D., Wu, C.C. & Weedman, D.W. 1980, ApJS, 43, 393.

Condon, J.J. 1974, AJ, 188, 279.

De Propris, R., Pritchett, C.J., Hartwick, F.D.A. & Hickson, P. 1993, AJ, 105, 1243.

Devereux, N.A. & Eales, S.A. 1989, ApJ, 340, 708.

Downes, D., Radford, J.E., Greve, A., Thum, C., Solomon, P.M., Wink, J.E. 1992, ApJ, 398, L25.

Downes, D. et al. 1999, A & A, 347, 809.

Dunne, L., Eales, S., Edmunds, M., Ivison, R., Alexander, P. & Clements, D. 2000, MNRAS, 315, 115.

Dunne, L., Clements, D. & Eales, S. 2000, MNRAS, in press (astro-ph 0002436).

Dwek, E. et al. 1998, *ApJ*, 508, 106.

Eales, S.A., Lilly, S., Gear, W., Dunne, L., Bond, J.R., Hammer, F., Le Fèvre, O. & Crampton, D. 1999, *ApJ*, 515, 518 (Paper I).

Eales, S.A. & Edmunds, M.G. 1996, *MNRAS*, 280, 1167.

Eales, S.A. & Edmunds, M.G. 1997, *MNRAS*, 286, 732.

Eales, S.A., Wynn-Williams, C.G. & Beichmann, C. 1988, *ApJ*, 328, 530.

Edmunds, M.G. & Phillipps, S. 1997, *MNRAS*, 292, 733.

Fabian, A.C. et al. 2000, *MNRAS*, 315, 8.

Feigelson, E.D. & Nelson, P.I. 1985, *ApJ*, 293, 192.

Fixsen, D.J., Dwek, E., Mather, J.C., Bennett, C.L. & Shafer, R.A. 1998, *ApJ*, 508, 123.

Flores, H. et al. 1999a, *A & A*, 343, 389.

Flores, H. et al. 1999b, *ApJ*, 517, 148.

Folkes, S. et al. 1999, *MNRAS*, 308, 459.

Fomalont, E.B., Windhorst, R.A., Kristian, J.A. & Kellerman, K.I. 1991, *AJ*, 102, 1258.

Gear, W.K., Lilly, S.J., Stevens, J.A., Clements, D.L., Webb, T.R., Eales, S.A. & Dunne, L., *MNRAS*, in press (Paper III), astro-ph 0007054.

Genzel, R. et al. 1998, *ApJ*, 498, 579.

Haehnelt, M.G., Natarajan, P. & Rees, M. 1998, *MNRAS*, 300, 817.

Helou, G., Soifer, B.T. & Rowan-Robinson, M. 1986, *ApJ*, 298, L7.

Holland, W.S. et al. 1999, *MNRAS*, 303, 659.

Hornschemeier, A.E. et al. 2000, *ApJ*, in press.

Hughes, D.H., Gear, W.K. & Robson, E.I. 1994, *MNRAS*, 270, 641.

Hughes, D.H. et al. 1998, *Nature*, 394, 241.

Jauncey, D.L. 1967, *Nature*, 216, 877.

Jenness, T. 1997, SURF - SCUBA user reduction facility. *Starlink User Note 216.1*.

Kawara, K. et al. 1998, *A & A*, 336, L9.

Lagache, G., Abergel, A., Boulanger, F., Désert, F.X. & Puget, J.-L. 1999, *A & A*, 344, 322.

Lagache, G., Puget, J.L. & Gispert, R. 1999, *Astronomy and Space Science*, in press (astro-ph 9910258).

La Valley, M., Isobe, T., & Feigelson, E.D. 1992, *Bulletin of the American Astronomical Society*, 24, 839.

Lilly, S., Eales, S.A., Gear, W., Hammer, F., Le Fèvre, O., Crampton, D., Bond, J.R. & Dunne, L., 518, 641 (Paper II).

Lilly, S., Le Fèvre, O., Crampton, D., Hammer, F. & Tresse, L. 1995, *ApJ*, 455, 50.

Lutz, D., Spoon, H.W.W., Rigopoulou, D., Moorwood, A.F.M. & Genzel, R. 1998, *ApJ*, 505, L103.

Magorrian, J. et al. 1998, *AJ*, 115, 2285.

Pagel, B. 1997, *Nucleosynthesis and Chemical Evolution of Galaxies* (CUP).

Peacock, J.A. et al. 2000, *MNRAS*, submitted (astro-ph 9912231).

Pettini, M., Kellogg, M., Steidel, C., Dickinson, M., Adelberger, K. & Giavalisco, M. 1998, *ApJ*, 508, 539.

Phillips, S. & Davies, J. 1991, *MNRAS*, 251, 105.

Puget, J.-L., Abergel, A., Bernard, J.-P., Boulanger, F., Burton, W.B., Desert, F.-X. & Hartmann, D. 1996, *A&A*, 308, L5.

Puget, J.L. et al. 1999, *A & A*, 345, 29p.

Richards, E.A. 1999, *ApJ*, 513, L9.

Richards, E.A. 2000, *ApJ*, 533, 611.

Rieke, G.H., Cutri, R.M., Black, R.H., Kailey, W.F., McAlary, C.W., Lebofsky, M.J. & Elston, R. 1985, *ApJ*, 290, 116.

Roche, N. and Eales, S.A. 1999, *MNRAS*, 307, 703.

Sanders, D.B. & Mirabel, I.F. 1996, *ARA&A*, 74, 749.

Saunders, W., Rowan-Robinson, M., Lawrence, A., Efstathiou, G., Kaiser, N., Ellis, R.S. & Frenk, C.S. 1990, *MNRAS*, 242, 318.

Scheuer, P.A.G. 1957, *Proc. Camb. Phil. Soc.*, 53, 764.

Schmitt, H.R., Kinney, A.L., Calzetti, D. & Bergmann, T.S. 1997, *AJ*, 114, 592.

Scott, D. et al. 2000, *A & A*, 357, L5.

Setti, G. & Woltjer, L. 1989, *A & A*, 224, L21.

Smail, I., Ivison, R.J. and Blain, A.W. 1997, *ApJ*, 490, L5.

Smail, I., Ivison, R., Blain, A. & Kneib, J.-P. 1998, *ApJ*, 507, L21.

Smail, I., Ivison, R.J., Owen, F.N. Blain, A.W. & Kneib, J.-P. 2000, *ApJ*, 528, 612.

Smith, H.E., Lonsdale, C.J., Lonsdale, C.J. & Diamond, P.J. 1998, *ApJ*, 493, L17.

Soifer, B.T, Boehmer, L., Neugebauer, G. & Sanders, D.B. 1989, *AJ*, 98, 766.

Steidel, C.C., Adelberger, K.L., Dickinson, M., Giavalisco, M., Pettini, M. & Kellogg, M. 1998, *ApJ*, 492, 428.

Steidel, C.C., Adelberger, K.L., Giavalisco, M., Dickinson, M. & Pettini, M. 1999, *ApJ*, 519, 1.

Williams, R.E. et al. 1996, *AJ*, 112, 1335.

Fig. 1.— Bolometric luminosity versus redshift for a source with an  $850\mu\text{m}$  flux density of 4 mJy and a dust temperature of 20, 30, 40, 50 and 60K. The dashed lines are for a universe with  $\Omega_0 = 0$  and the continuous lines for  $\Omega_0 = 1$ . The thick dashed line shows the bolometric luminosity of the archetypical ULIRG, Arp 220.

Fig. 2.— Images of the  $14^h$  field. Each image is approximately 6.9 times  $6.4 \text{ arcmin}^2$ . An edge region containing artefacts, a well-known phenomenon of the SCUBA map-making process, has been removed. The raw image convolved with a Gaussian of size (FWHM) 10 arcsec, which degrades the resolution slightly (from 14 to 18 arcsec) but reveals the faint sources more clearly, is shown in (a). The image after all the 19 sources have been removed is shown in (b). An artificial image showing the 19 sources at the 14-arcsec resolution of the telescope is shown in (c). The noise image described in §4.1 is shown in (d). On this image, the two dashed contours indicate noise levels of 0.8 and 0.9 mJy; the continuous lines indicate noise levels of 1.1, 1.2, 1.3...mJy.

Fig. 3.— Integral source counts at  $850\mu\text{m}$ . The key to the symbols is shown in the figure. The error bars in each case are Poisson error bars and, as the counts are integral counts, the error bars for a particular survey are not independent.

Fig. 4.— Results of the Monte-Carlo simulations of the  $14^h$  field described in §4.3. The top row of plots is for the simulations in which the artificial images only contain sources and the bottom row is for the images which also contain noise. The lefthand plot in both rows shows the true flux of the source (input flux) versus the flux measured by the source-detection algorithm (output flux). The sloping line shows where the input and output fluxes are the same and the dashed lines indicate notional catalog limits of 3 mJy. The middle plot in each row shows the difference in arcsec between the true position of a source and the position determined by the source-detection algorithm plotted against output flux. The righthand plot shows this positional difference plotted against the ratio of the output flux to the input flux (the ‘flux boost’). For clarity, in the bottom row only sources with either input or output fluxes brighter than 3 mJy have been included.

Fig. 5.— The predicted ratio of  $850\mu\text{m}$  to 1.4 GHz flux for star-forming galaxies from Dunne, Clements and Eales (2000). The thick line shows the average value of this ratio and the thin lines show the  $\pm 1\sigma$  dispersion. The measured ratios are shown for all SCUBA galaxies with spectroscopic redshifts and radio detections (this paper; Barger, Cowie & Richards 2000; Smail et al. 2000).

Fig. 6.— Redshift histograms for (a) the sample of Smail et al. (2000), (b) the sample of Barger, Cowie and Richards (2000) with  $S_{850\mu\text{m}} > 6\text{mJy}$ , (c) the sources in the  $14^h$  field. The hatched parts of the histograms show the redshift limits obtained using the radio method described in §6.2. The redshift ‘measurements’ are either estimates from the radio technique or in a few cases are spectroscopic redshifts.

Fig. 7.— The ratio of  $15\mu\text{m}$  flux to  $850\mu\text{m}$  flux for the galaxies in the  $14^h$  field detected in either this survey or in the  $15\mu\text{m}$  survey of Flores et al. (1999b). The two measurements are for the two galaxies detected in both surveys. The lower limits are for the galaxies with spectroscopic redshifts

in Catalogue 1 of Flores et al. The upper limits are for the sources detected at  $850\mu\text{m}$  which were not detected at  $15\mu\text{m}$ ; none of these has a spectroscopic redshift, so the redshift or redshift limit estimated from the radio method has been used (§6.2). The lines show the predictions of the models described in the text (§6.3): the continuous line is the prediction of the high-extinction starburst (SBH) model; the dot-dash line is for the spiral galaxy model; and the dashed line is the prediction of the model based on the spectral energy distribution of Arp 220.

Fig. 8.— The ratio of  $450\mu\text{m}$  flux to  $850\mu\text{m}$  flux redshift for the galaxies detected in either the  $14^h$  field (this paper) or in the  $3^h$  and  $10^h$  fields (Paper I). Only objects for which there is some redshift information (a spectroscopic redshift or an estimated redshift or limit) have been plotted: the filled symbols show galaxies which have spectroscopic redshifts; the squares show galaxies which have estimated redshifts, either from the radio method (§6.2) or from optical/IR colours (Paper II); the circles show galaxies for which there are redshift limits estimated using the radio technique. The horizontal line shows the  $3\sigma$  upper limit on the average  $450\mu\text{m}$  to  $850\mu\text{m}$  flux ratio for the sources detected in the  $850\mu\text{m}$  survey, derived by summing the  $450\mu\text{m}$  emission at the position of each  $850\mu\text{m}$  source (§4.1). The lines show the predictions of the models described in the text (§6.3): the continuous line is the prediction of the high-extinction starburst (SBH) model; the dot-dash line is for the spiral galaxy model; the dashed line is the prediction of the model based on the spectral energy distribution of Arp 220; and the dotted line is the prediction of the model based on the spectral energy distribution of IRAS 10214+4724.

Fig. 9.— Submillimetre properties predicted for the Lyman-break galaxies by the model described in the text (§7.1), which is based on the submillimetre detection of this population by Peacock et al. (2000). The upper plot shows the predicted submillimetre background from this population on the assumption of a dust temperature of 20K (continuous line) or 40K (dashed line). The thick dot-dash line shows the measured submillimetre background (Fixsen et al. 1998). The bottom plot shows the predicted  $850\mu\text{m}$  source counts (continuous line; the predicted counts do not depend on dust temperature). The symbols show the measured counts and the key is the same as in Figure 3.

Fig. 10.— Predictions of the evolution models described in the text (§7.2). In these models the bolometric luminosity of the dust in a galaxy is assumed to vary as  $(1+z)^p$  at  $z < z_t$  and as  $(1+z)^q$  at  $z > z_t$ . Each plot is for a different value of  $z_t$  and shows  $p$  plotted against  $q$ . The continuous line in each plot encloses the models which give an acceptable fit to the  $850\mu\text{m}$  source counts and the submillimetre background ('acceptable' is defined in the text) and also predict that the fraction of sources with  $S_{850\mu\text{m}} > 4\text{mJy}$  that have  $z < 2$  falls between 20 and 80%, our admittedly subjective estimate of how uncertain this quantity is. The dashed line shows the additional region of acceptability if this redshift criterion is ignored. The greyscale further shows the percentage of sources predicted to lie at  $z < 2$ ; the ten levels of the greyscale are: 0 to 10%, 10-20%, 20-30%, 30-40%, 40-50%, 50-60%, 60-70%, 70-80%, 80-90%, 90-100%. This montage is for a maximum redshift of 5.0 and a density constant ( $\Omega_0$ ) of 1.

Fig. 11.— The same as Figure 10 except that the dust temperatures of all galaxies are assumed to increase by a factor of 1.5 at  $z = z_t$ . Note that there are no acceptable models for  $z_t = 1$ .

Fig. 12.— The same as Figure 10 except that the dust temperatures of all galaxies are assumed to increase by a factor of 1.5 at  $z = z_t$  and the maximum redshift has been raised to 10.

Fig. 13.— Bolometric luminosity density in the universe versus redshift for all models which are in agreement with the observations. The horizontal lines show the optical/UV luminosity density in the universe at  $z = 0$  and  $z \sim 3$  estimated using the methods described in the text.

Fig. 14.— The fraction of stars that have formed by a redshift  $z$  for all the models which are in agreement with the observations.

Table 1. Observing Log

Date	Integration Time	$\tau_{850\mu m}$	$\tau_{450\mu m}$
1998 March 5	9600s	0.21-0.25	1.11-1.39
1998 March 6	12160s	0.13-0.14	0.57-0.68
1998 March 7	12160s	0.17-0.23	0.84-1.23
1998 March 8	9600s	0.20-0.22	1.03-1.16
1998 March 9	9600s	0.20-0.22	1.09-1.20
1998 March 10	12800s	0.16-0.17	0.72-0.77
1998 March 11	9600s	0.17-0.17	0.83-0.85
1998 March 12	9600s	0.18-0.19	0.89-0.90
1998 March 13	12800s	0.20-0.22	1.19-1.23
1998 March 15	9600s	0.22-0.29	1.20-1.65
1998 June 16	11392s	0.20-0.25	1.24-1.53
1998 June 17	9600s	0.17-0.18	0.88-0.95
1998 June 18	12800s	0.23-0.29	1.21-1.73
1998 June 19	8320s	0.26-0.26	1.34-1.47
1999 Jan 11	14976s	0.13-0.14	0.64-0.76
1999 Jan 12	14080s	0.27-0.36	1.79-3.00
1999 March 6	4992s	0.27-0.33	1.71-2.11
1999 May 25	16000s	0.32-0.47	2.36-3.25
1999 May 26	16000s	0.33-0.41	2.23-3.06
1999 May 27	11520s	0.18-0.20	0.94-1.02

Note. — Col. 1: date. Col. 2: total integration time in seconds. Col. 3: the range of optical depth at the zenith at 850  $\mu m$  for these observations. Col. 4: same as for the previous column but at 450  $\mu m$ .

Table 2. Catalog

Name	Old name	RA and Dec (J2000.0)	S/N	$S_{850\mu\text{m}}/\text{mJy}$	$S_{450\mu\text{m}}/\text{mJy}$
CUDSS 14.1 <sup>†</sup>	14A	14 17 40.25 52 29 06.5	10.1	$8.7 \pm 1.0$	$2.7 \pm 13.3$
CUDSS 14.2 <sup>†</sup>	14B	14 17 51.7 52 30 30.5	6.3	$5.5 \pm 0.9$	$22.9 \pm 12.0$
CUDSS 14.3 <sup>†</sup>	...	14 18 00.5 52 28 23.5	5.4	$5.0 \pm 1.0$	$-1.0 \pm 8.3$
CUDSS 14.4 <sup>†</sup>	...	14 17 43.35 52 28 14.5	5.3	$4.9 \pm 0.9$	$-9.8 \pm 15.7$
CUDSS 14.5 <sup>†</sup>	...	14 18 07.65 52 28 21	4.5	$4.6 \pm 1.0$	$12.6 \pm 7.5$
CUDSS 14.6	...	14 17 56.6 52 29 07	4.2	$4.1 \pm 1.0$	$-25.0 \pm 17.1$
CUDSS 14.7 <sup>†</sup>	...	14 18 01.1 52 29 49	3.2	$3.2 \pm 0.9$	$3.1 \pm 11.7$
CUDSS 14.8 <sup>†</sup>	14E	14 18 02.7 52 30 15	4.0	$3.4 \pm 0.9$	$-5.5 \pm 11.2$
CUDSS 14.9 <sup>†</sup>	...	14 18 09.0 52 28 04	4.1	$4.3 \pm 1.0$	$-2.6 \pm 7.5$
CUDSS 14.10 <sup>†</sup>	...	14 18 03.9 52 29 38.5	3.5	$3.0 \pm 0.8$	$-6.4 \pm 11.7$
CUDSS 14.11	...	14 17 47.1 52 32 38	3.5	$4.5 \pm 1.3$	$-12.7 \pm 18.5$
CUDSS 14.12	...	14 18 05.3 52 28 55.5	3.4	$3.4 \pm 1.0$	$7.4 \pm 8.6$
CUDSS 14.13 <sup>†</sup>	...	14 17 41.2 52 28 25	3.4	$3.3 \pm 1.0$	$-1.4 \pm 15.2$
CUDSS 14.14	...	14 18 08.65 52 31 03.5	3.3	$4.6 \pm 1.3$	$-22.0 \pm 15.2$
CUDSS 14.15	...	14 17 29.3 52 28 19	3.1	$4.8 \pm 1.5$	$-22.3 \pm 25.2$
CUDSS 14.16 <sup>†</sup>	...	14 18 12.25 52 29 20	3.7	$4.7 \pm 1.4$	.....
CUDSS 14.17 <sup>†</sup>	...	14 17 25.45 52 30 44	3.3	$6.0 \pm 2.1$	$35.7 \pm 41.3$
CUDSS 14.18 <sup>†</sup>	14F	14 17 42.25 52 30 26.5	3.0	$2.6 \pm 0.9$	$24.2 \pm 10.4$
CUDSS 14.19 <sup>†</sup>	...	14 18 11.5 52 30 04	3.0	$3.9 \pm 1.3$	$4.4 \pm 18.8$

Note. — Col. 1: Name of source. A dagger indicates there is a note about this source in the text. Col. 2: Name of source in Paper I. Col. 3: Position of source. Col. 4: Signal-to-noise with which the source was detected at 850 $\mu\text{m}$ . Cols 5 & 6: Flux density at 850 and 450  $\mu\text{m}$  (measured using the methods described in §4.1). The error does not include the calibration error, which we estimate is  $\simeq 5\%$  at 850  $\mu\text{m}$  and  $\simeq 20\%$  at 450  $\mu\text{m}$ .

Table 3. Other Sources

Name	Old name	RA and Dec (J2000.0)	S/N	$S_{850\mu\text{m}}/\text{mJy}$	$S_{850\mu\text{m}}/\text{mJy}$
CUDSS 14.20	14D	14 18 02.3 52 30 51.5	2.9	$2.5\pm0.9$	$3.2\pm0.9$
CUDSS 14.21	14C	14 17 33.8 52 30 49	2.4	$2.3\pm1.0$	$3.8\pm1.1$

Note. — Col. 1: Name of source. Col. 2: Name of source in Paper I. Col. 3: Position of source. Col. 4: Signal-to-noise with which the source was detected at  $850\mu\text{m}$ . Col. 5: Flux density at  $850\mu\text{m}$ . Col. 6: Flux density at  $850\mu\text{m}$  from Paper I.

Table 4. SCUBA/ISO Associations

CUDSS	ISO	CFRS	RA and Dec (J2000.0)	d	p
14.13	0	14.1157	14 17 41.81 52 28 23.0	5.9	0.03
14.17	195	14.1569	14 17 24.36 52 30 46.45	10.3	0.08
14.18	5	14.1139	14 17 42.04 52 30 25.7	2.1	0.0036

Note. — Col. 1: Name of SCUBA source. Col. 2: Name of ISO source using the nomenclature of Flores et al. (1999b). Col. 3: Name of galaxy associated with the ISO source using the standard CFRS nomenclature (Flores et al. 1999b). Col. 4: Position of the galaxy in J2000 coordinates. Col. 5: Distance in arcsec between SCUBA position and optical position. Col. 6: Probability of an unrelated ISO source falling closer to the SCUBA source than this distance.

Table 5. SCUBA/Radio Associations

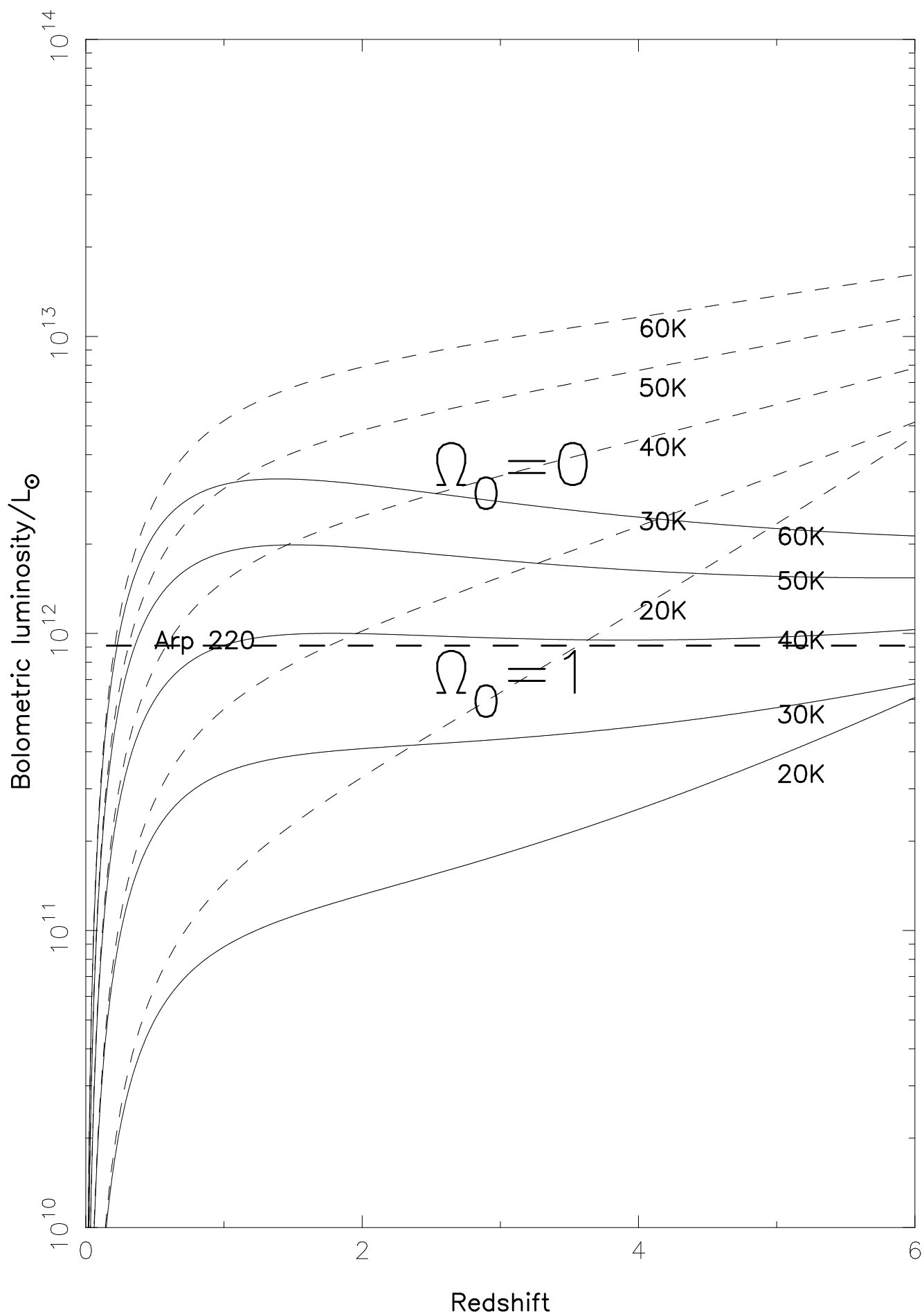
CUDSS	Radio	RA and Dec (J2000.0)	d	p	$S_{5\text{GHz}}$	$\alpha$	$z_{est}$	$z_{act}$
14.1	15V18	14 17 40.32 52 29 05.9	0.9	$6.0 \times 10^{-4}$	44.0	0.2	$2.2 \pm 0.5$	...
14.2	....	.....	...	...	<19	...	$>1.95$	...
14.3	15V53	14 18 00.5 52 28 20.8	2.7	$8.6 \times 10^{-3}$	30.1	0.9	$1.3 \pm 0.3$	...
14.4	....	.....	...	...	<15	...	$>2.1$	...
14.5	....	.....	...	...	<12	...	$>2.2$	...
14.6	....	.....	...	...	<12	...	$>2.1$	...
14.7	....	.....	...	...	<15	...	$>1.7$	...
14.8	....	.....	...	...	<18	...	$>1.6$	...
14.9	15V67	14 18 09.03 52 28 03	1.0	$1.1 \times 10^{-3}$	46.1	-0.2	$2.0 \pm 0.5$	...
14.10	....	.....	...	...	<18	...	$>1.5$	...
14.11	....	.....	...	...	(<83)	...	$>1.3$	...
14.12	....	.....	...	...	<12	...	$>1.9$	...
14.13	....	14 17 40.67 52 28 24.6	4.9	$2.1 \times 10^{-2}$	15	...	$2.1 \pm 0.5$	...
	15V23	14 17 41.81 52 28 23.4	5.8	$2.9 \times 10^{-3}$	53.6	0.3	$1.2 \pm 0.3$	1.15
14.14	....	.....	...	...	<26	...	$>1.5$	...
14.15	....	.....	...	...	(<75)	...	$>1.4$	...
14.16	....	.....	...	...	<15	...	$>2.0$	...
14.17	....	.....	...	...	(<49)	...	$>2.0$	...
14.18	15V24	14 17 42.08 52 30 25.2	2.0	$2.4 \times 10^{-4}$	78.9	0.5	$0.7 \pm 0.2$	0.66
14.19	....	.....	...	...	<16	...	$>1.8$	...

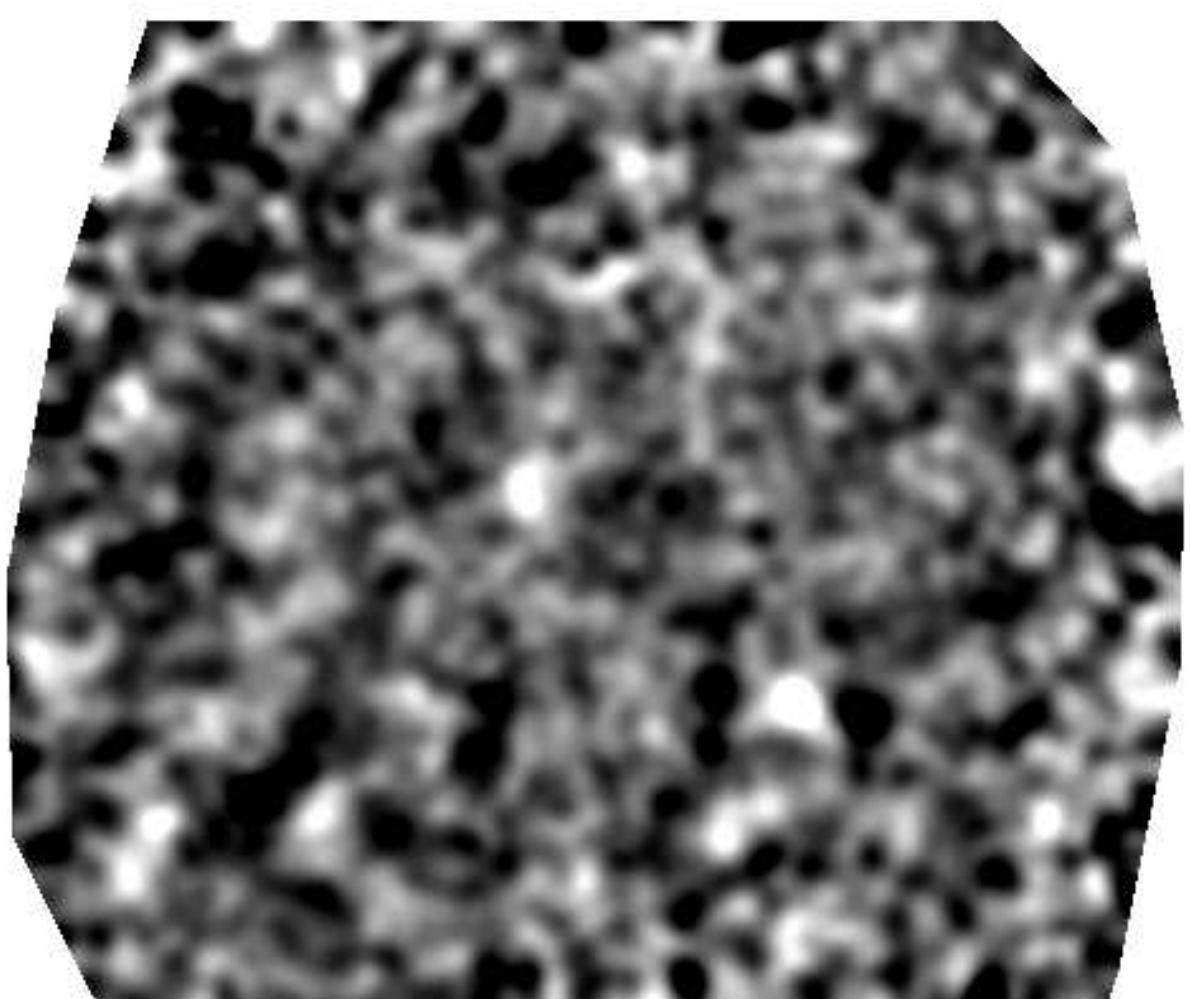
Note. — Col. 1: Name of SCUBA source. Col. 2: Name of radio source (Fomalont et al. 1991). Col. 3: Position of radio source. Col. 4: Distance in arcsec between SCUBA and radio positions. Col. 5: Probability of a radio source lying within this distance of the SCUBA source by chance. Col. 6: Flux density at 5 GHz in  $\mu\text{Jy}$ . CUDSS 14.11, 14.15 and 14.17 are outside the useable region of the 5-GHz map, so for these sources the radio upper limits are the  $3\sigma$  upper limits obtained from the re-reduced 1.5GHz map (see text). Col. 7: Radio spectral index,  $\alpha$ , from Fomalont et al. (1991), defined such that flux  $\propto$  frequency $^{-\alpha}$ . Col. 8: Redshift estimated from the ratio of 850 $\mu\text{m}$  to radio flux (see text). Col. 9: Spectroscopic redshift.

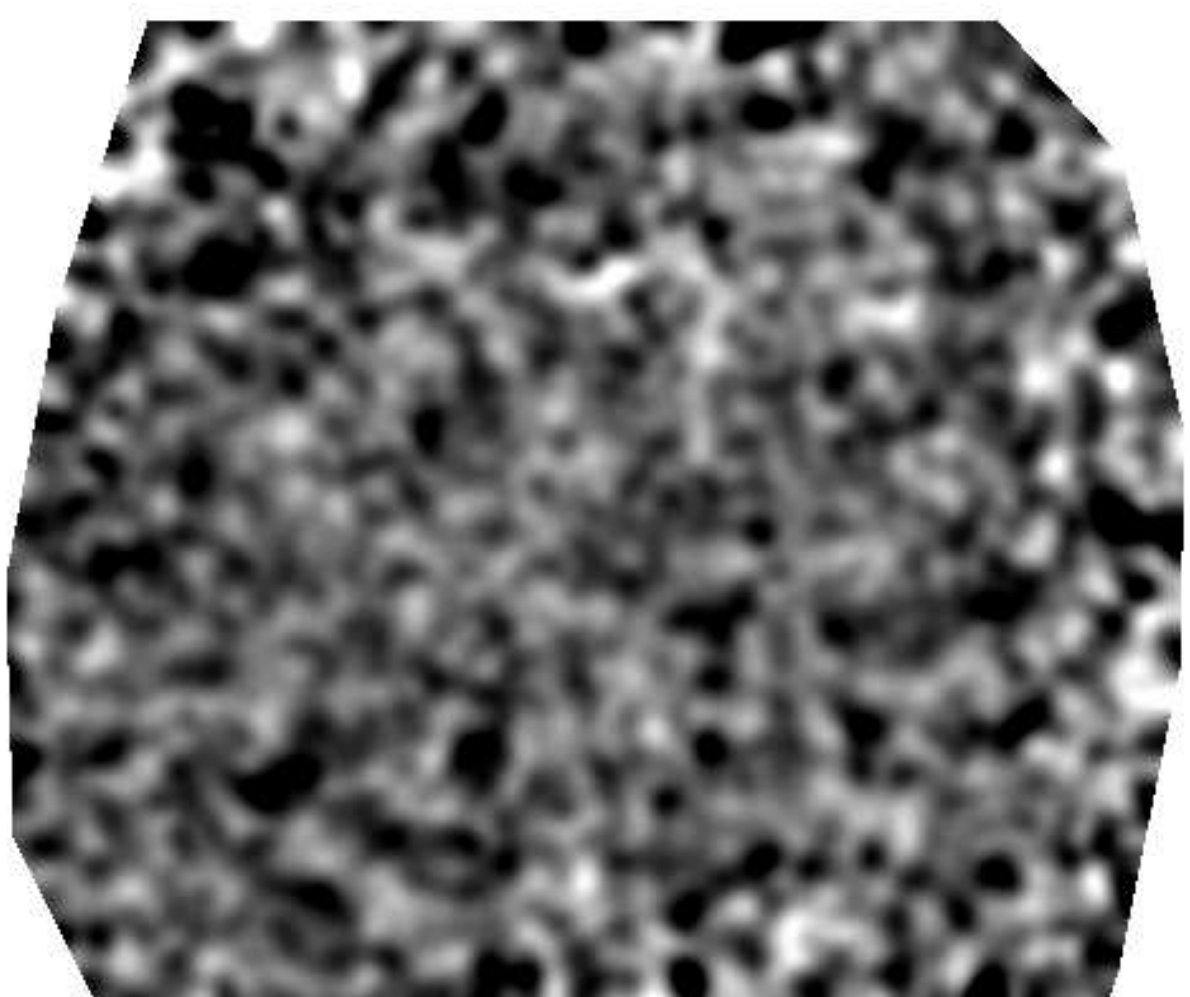
Table 6. Redshift Distributions

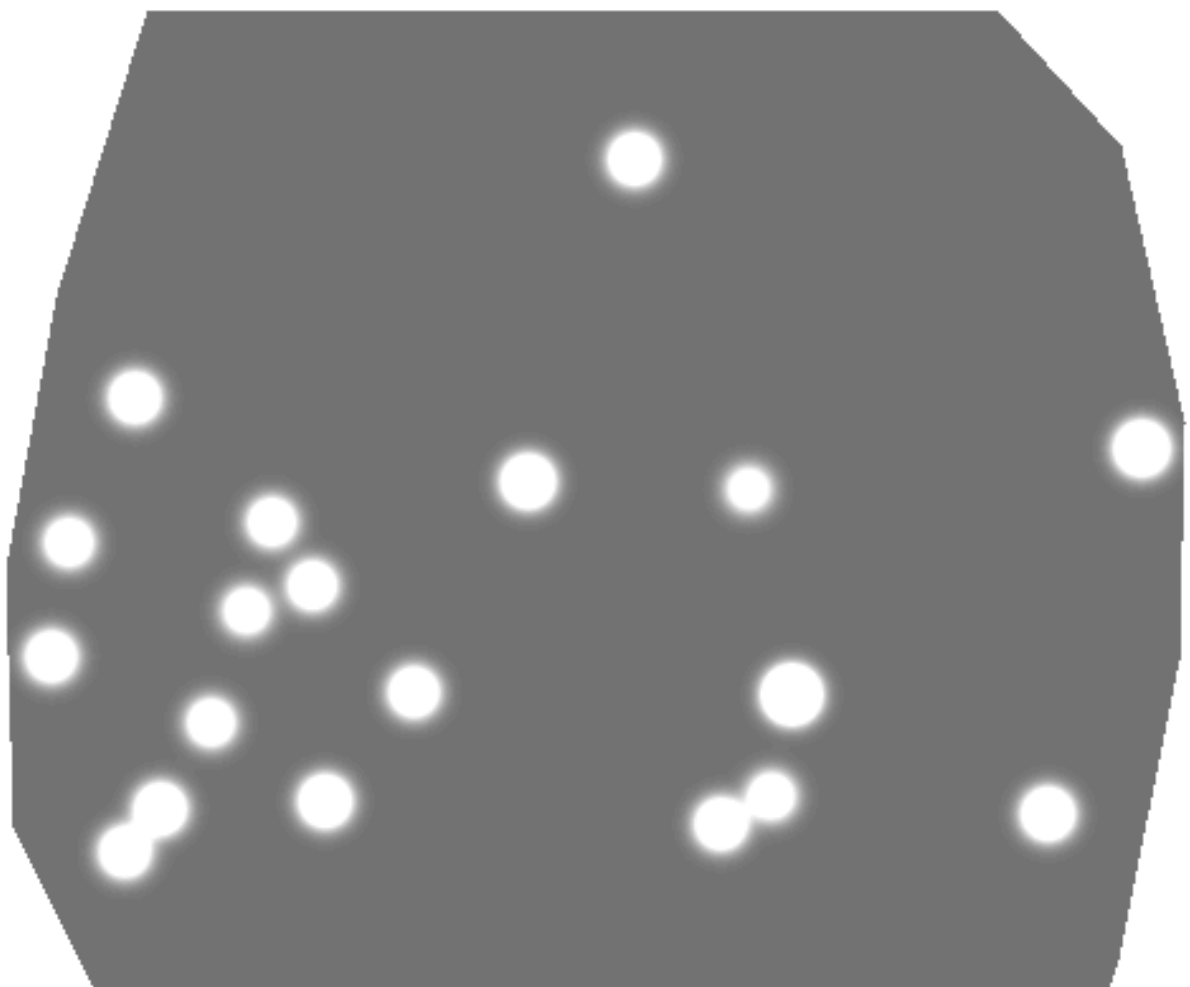
Sample	sources	$z_{spect}$	$z_{phot}$	Mean $z$	Median $z$	95% limits
CUDSS 14 <sup>h</sup>	19	2	3	1.96±0.15	2.05	undefined
Clusters	16	4	5	2.70±0.39	2.52	1.59,3.43
HFF	7	0	5	2.51±0.81	1.5	1.15,4.0
combined	42	6	13	2.81±0.36	2.41	1.94,3.48

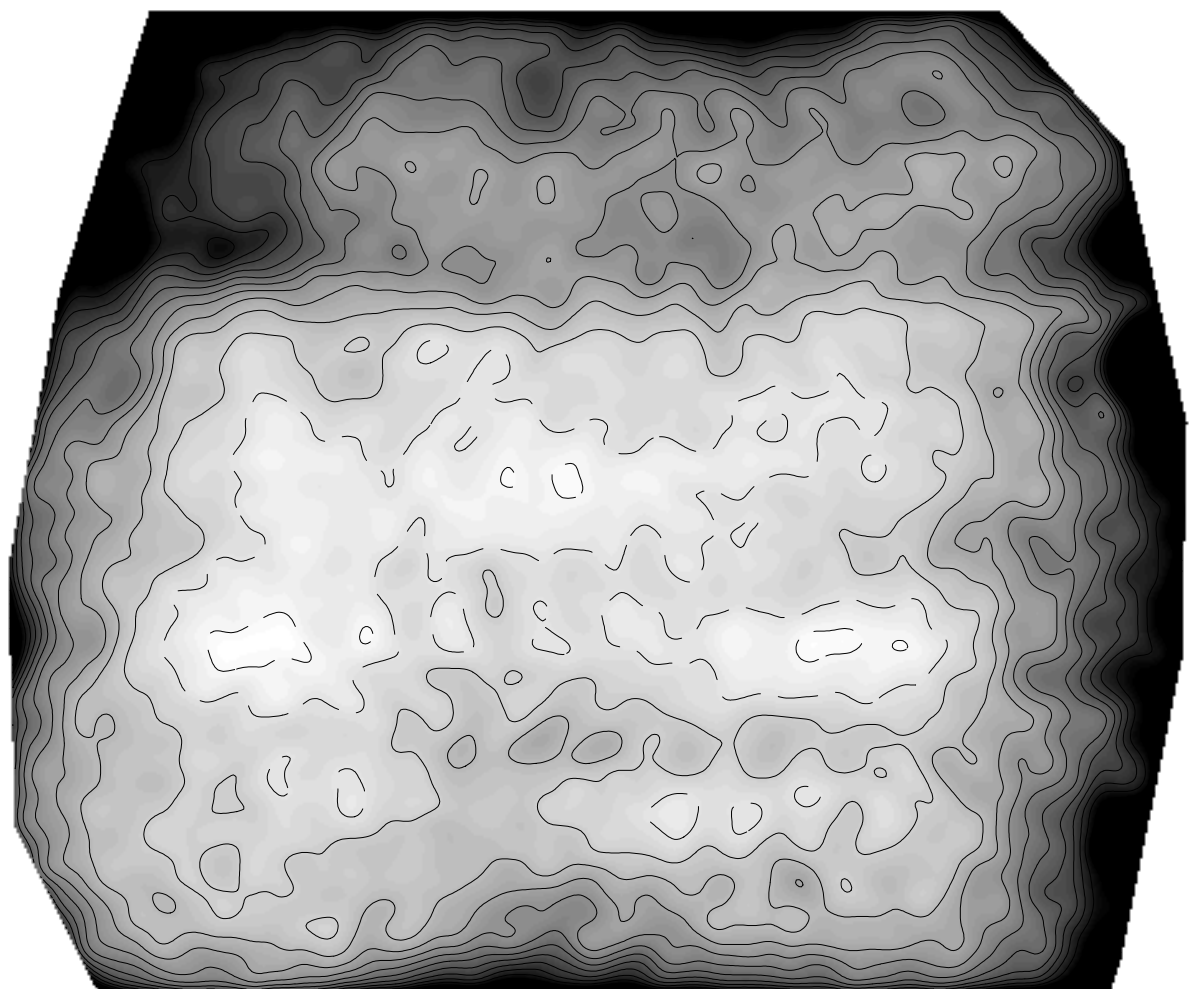
Note. — Col. 1: Name of sample with the following key: CUDSS 14<sup>h</sup>—this paper; Clusters—sample from Smail et al. (2000); HFF—sample from Barger, Cowie & Richards (2000); combined—all of the above samples together. Col. 2: Number of sources in the sample. Col. 3: Number of sources with spectroscopic redshifts; Col. 4: Number of sources with photometric redshifts but not a spectroscopic redshift. Col. 5: Mean redshift and error estimated using the Kaplan-Meier estimator; Col. 6—Median redshift; Col. 7—95% confidence interval for the median.

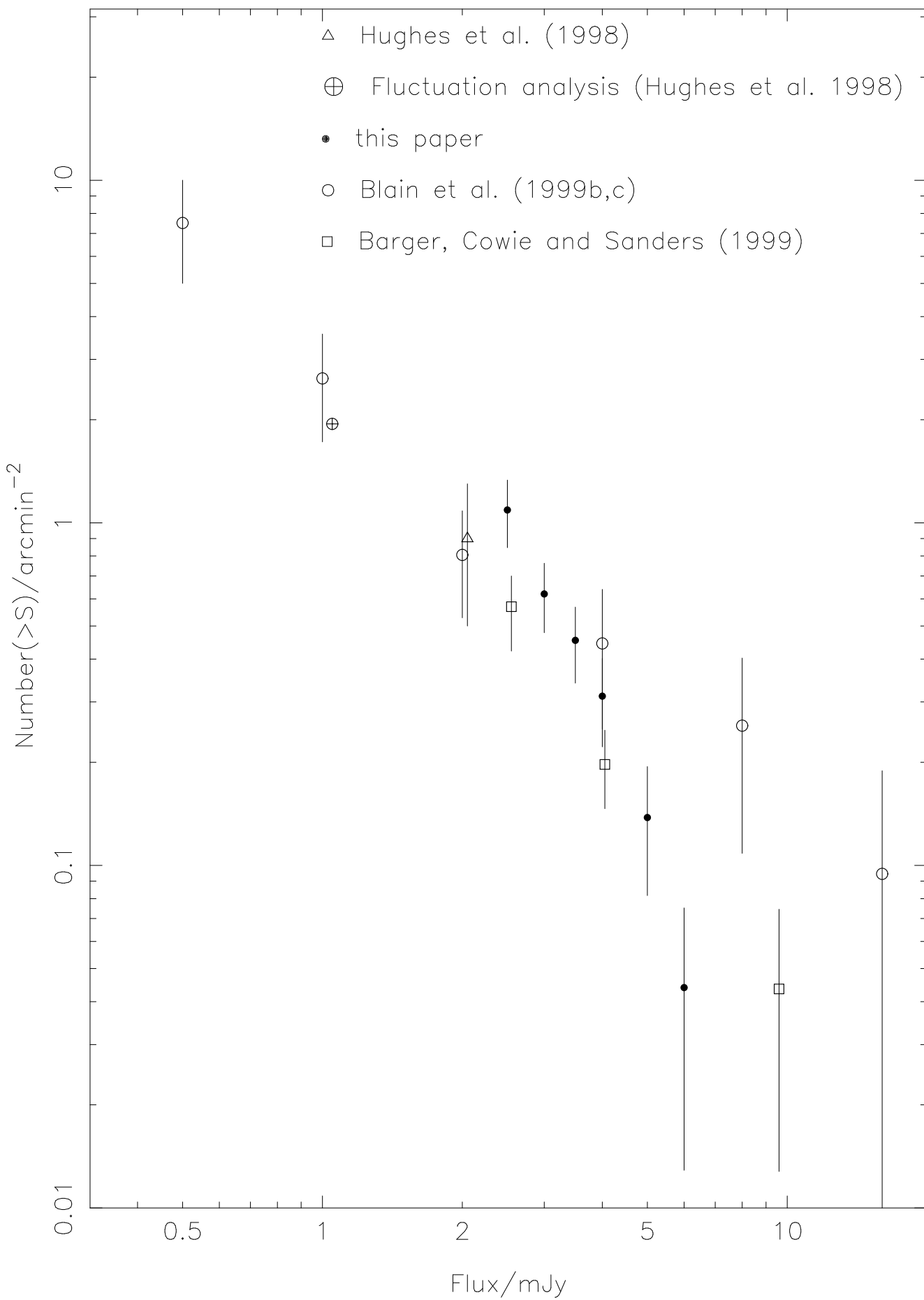


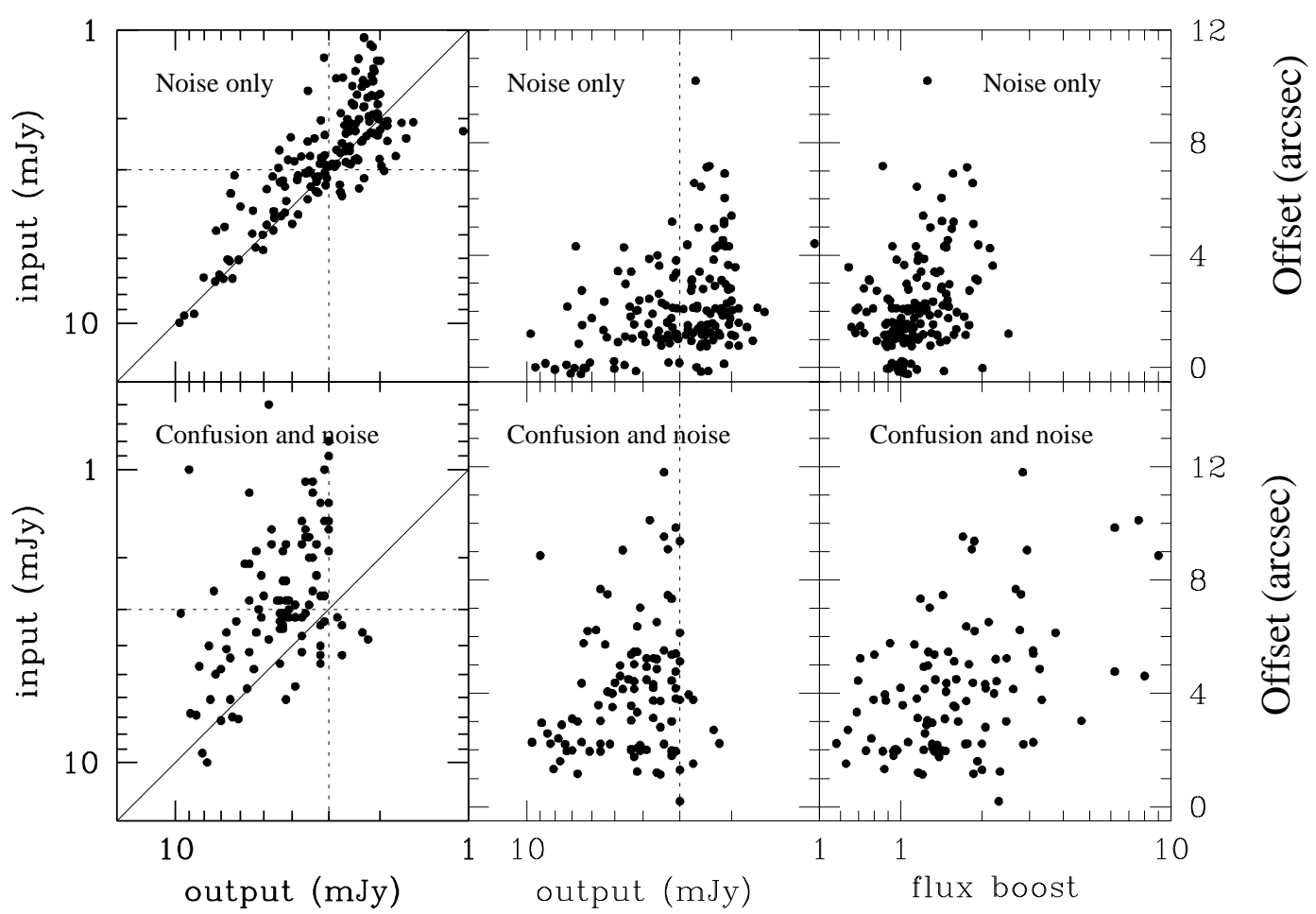


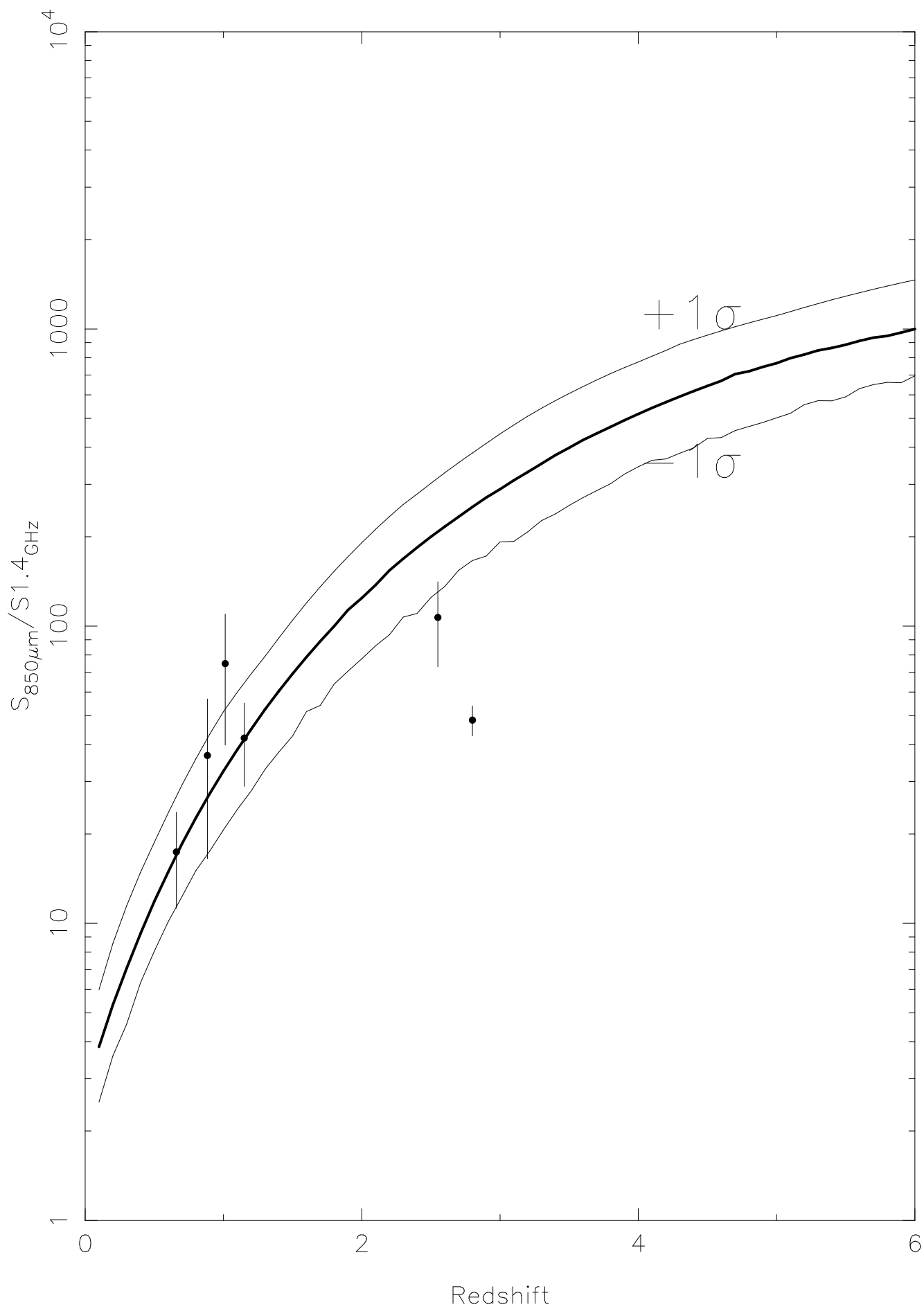


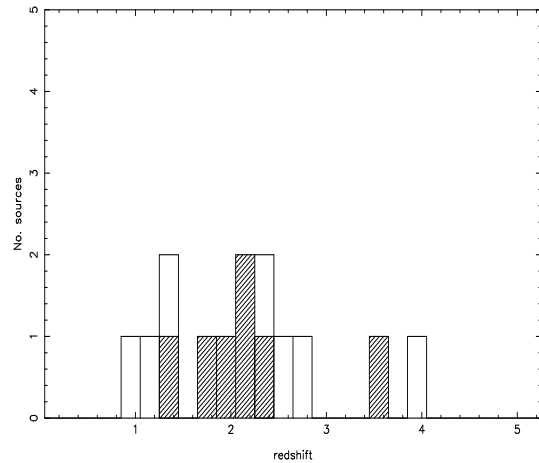




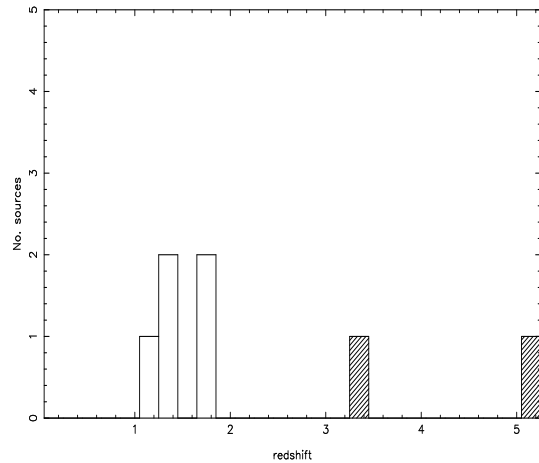




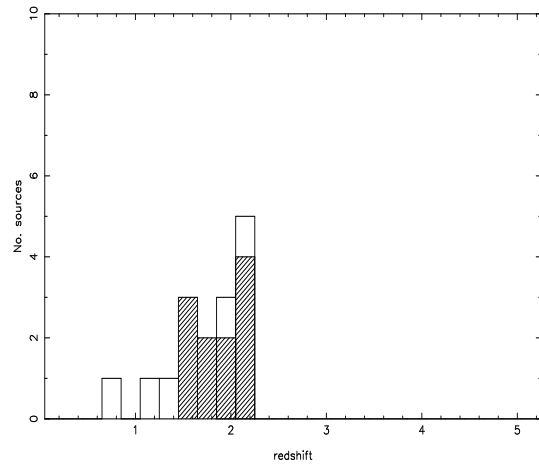




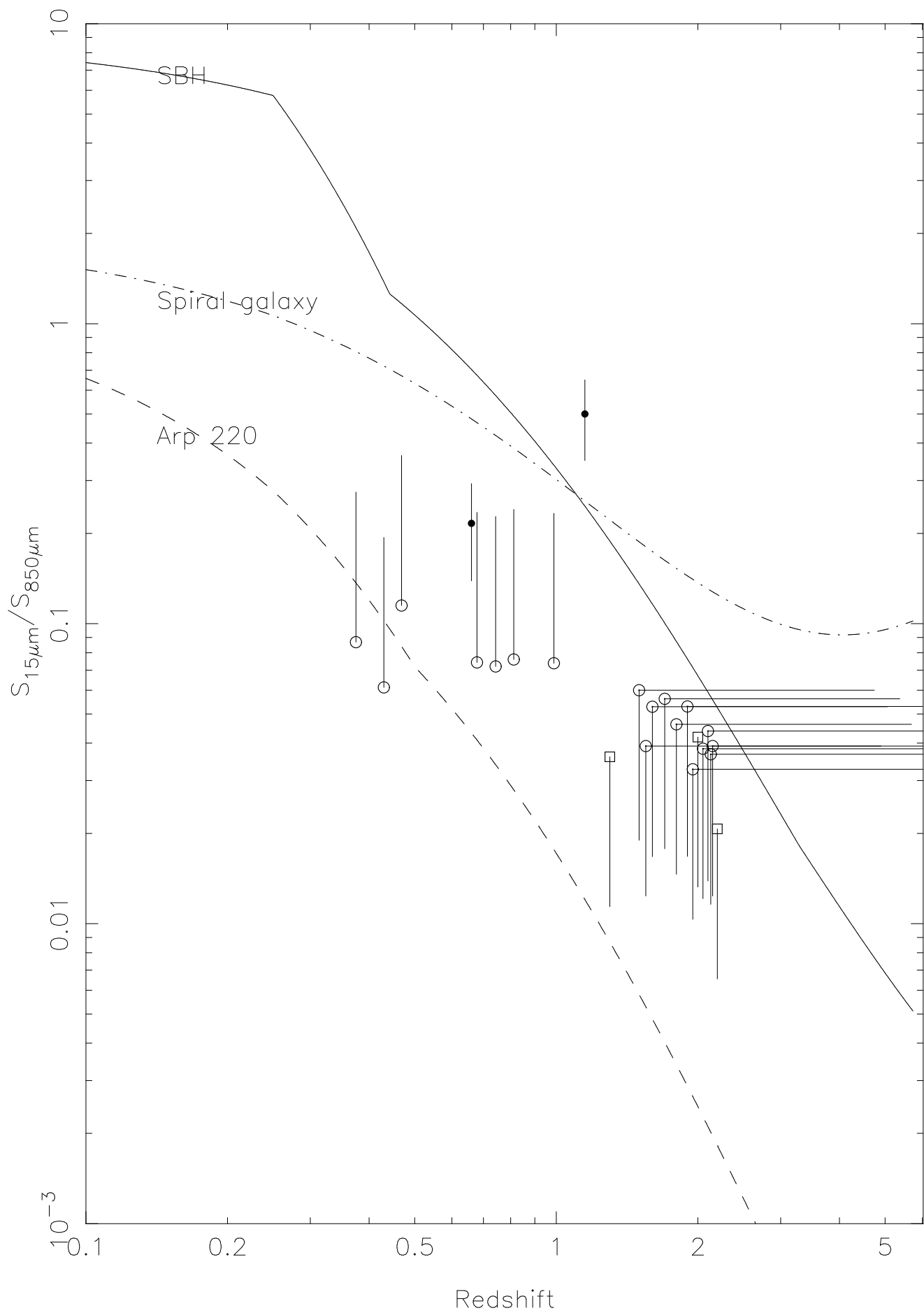
(a) Smail

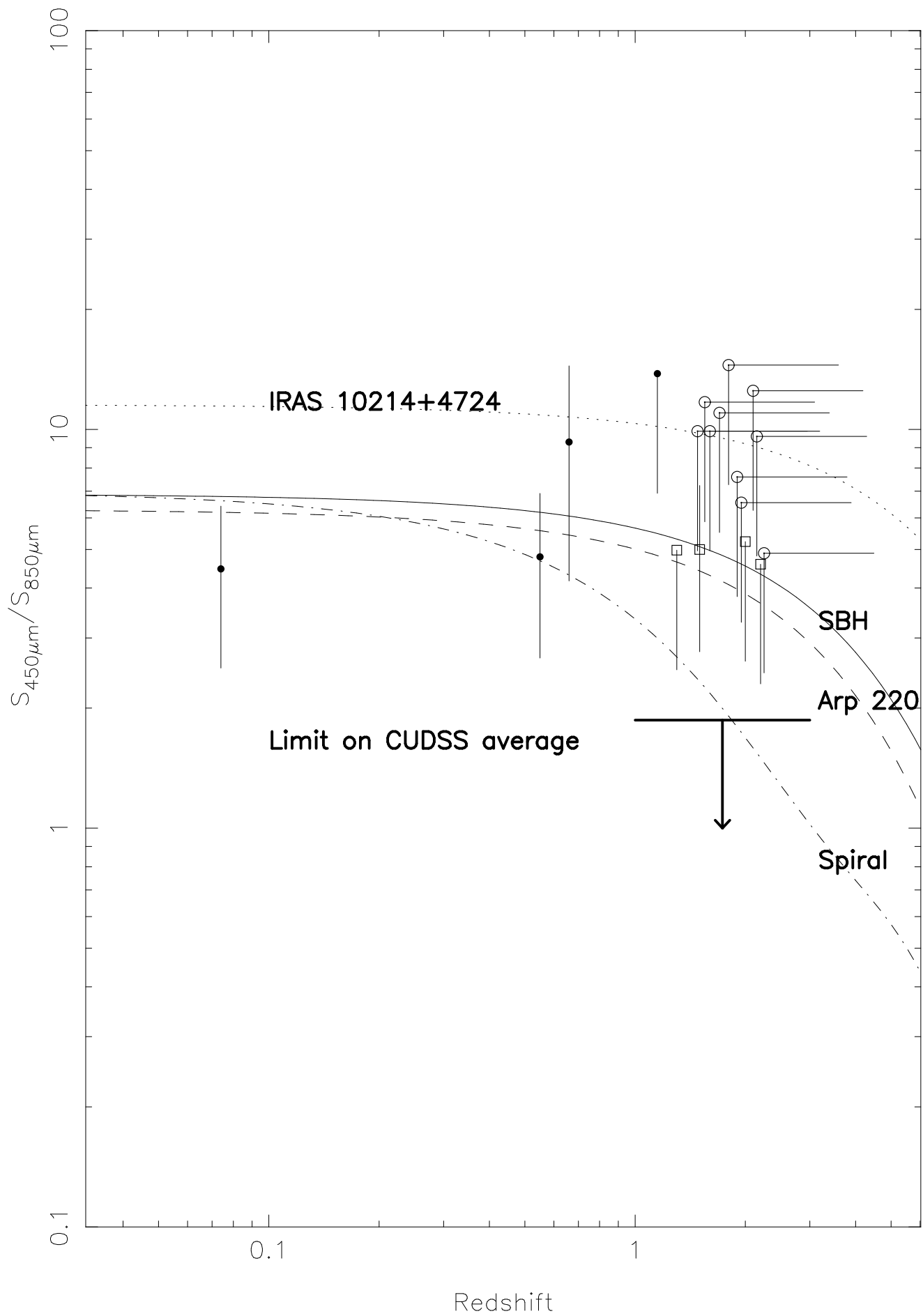


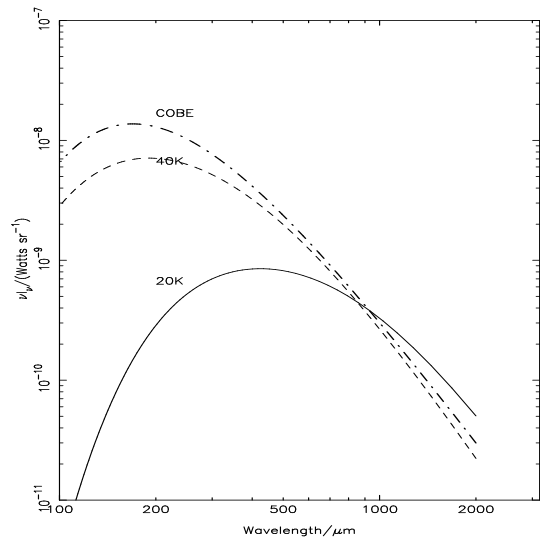
(b) Barger



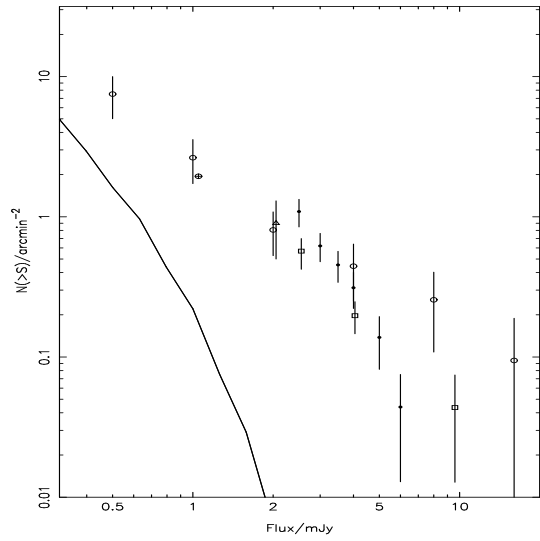
(c) CUDSS



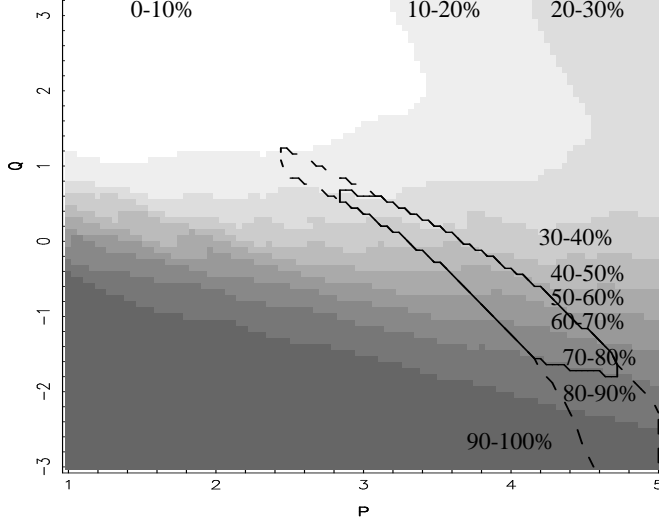




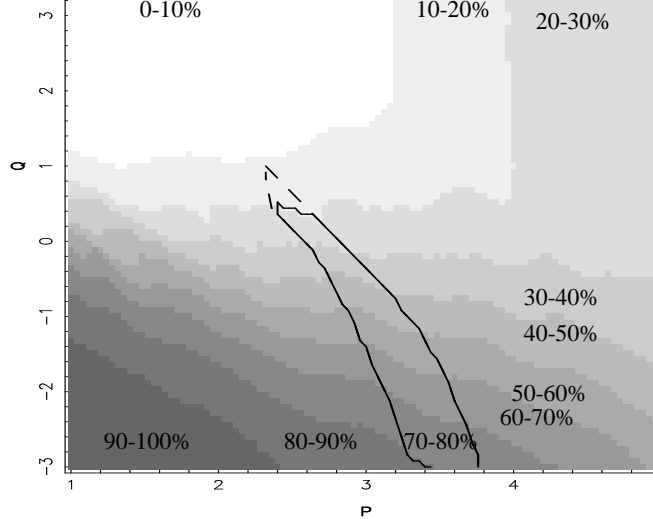
(a) Background



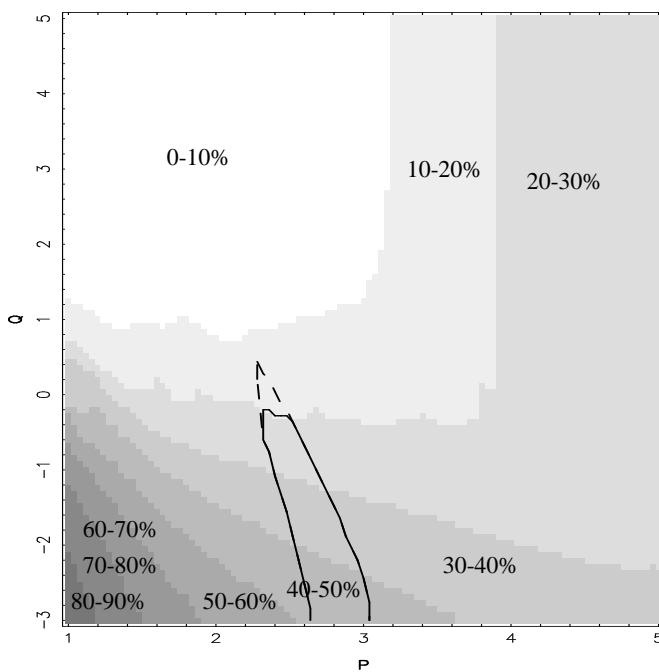
(b) 850\$\mu\text{m}\$ counts



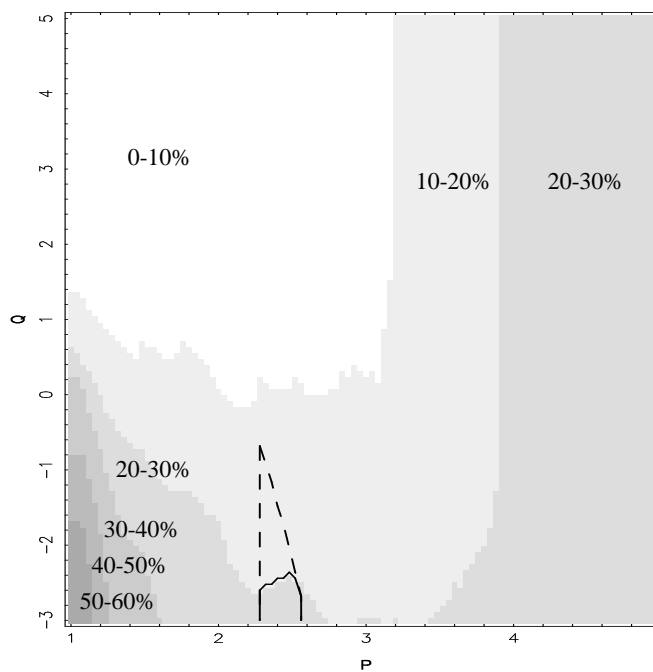
(a)  $z_t = 1.0$



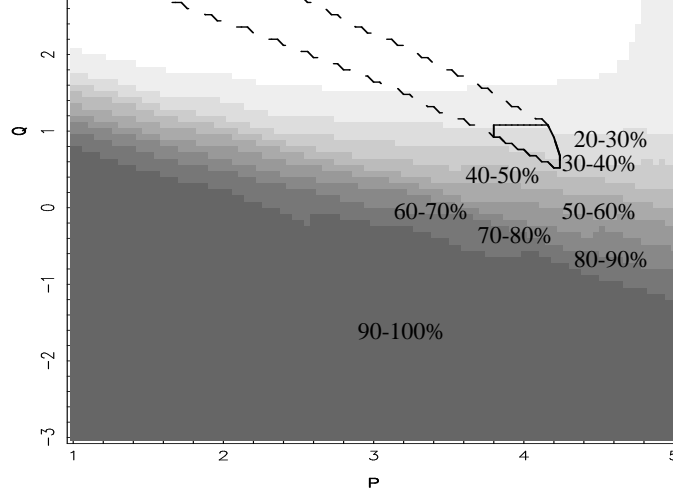
(b)  $z_t = 1.5$



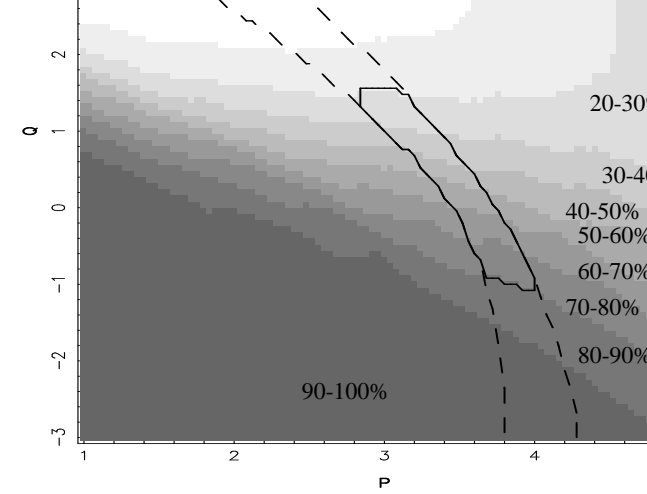
(c)  $z_t = 2.0$



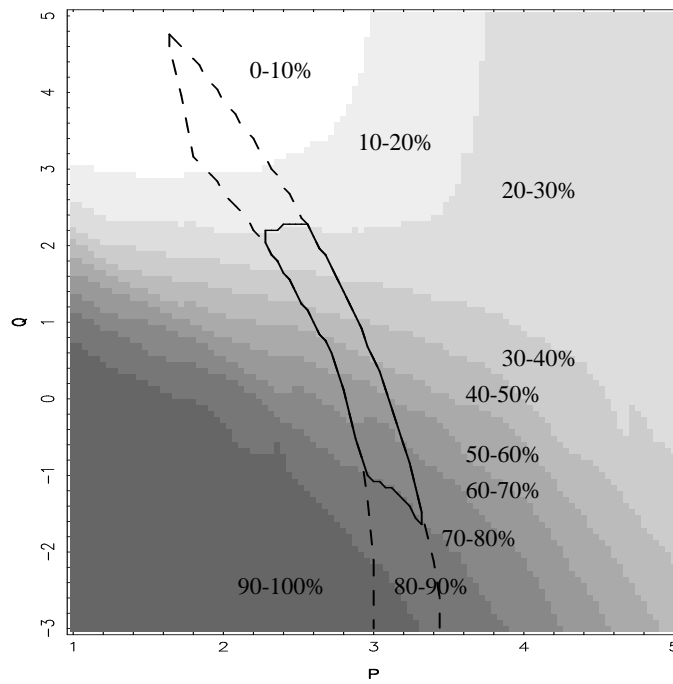
(d)  $z_t = 2.5$



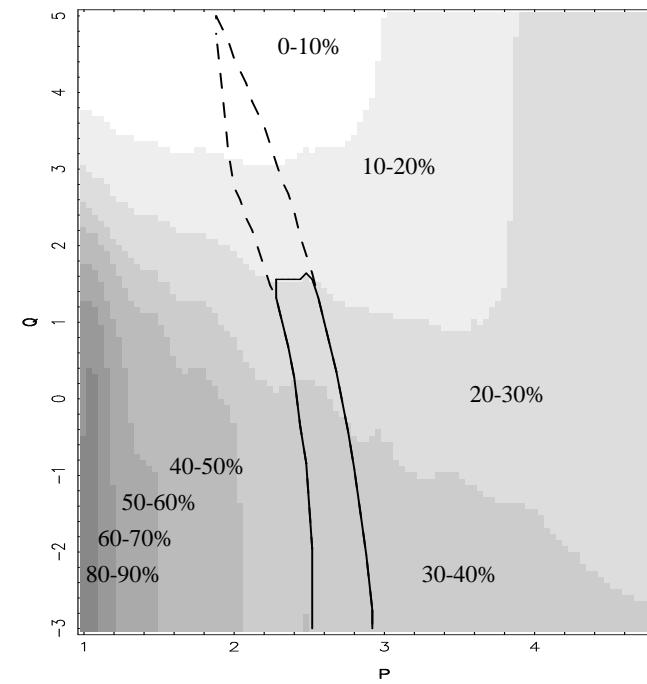
(a)  $z_t = 1.0$



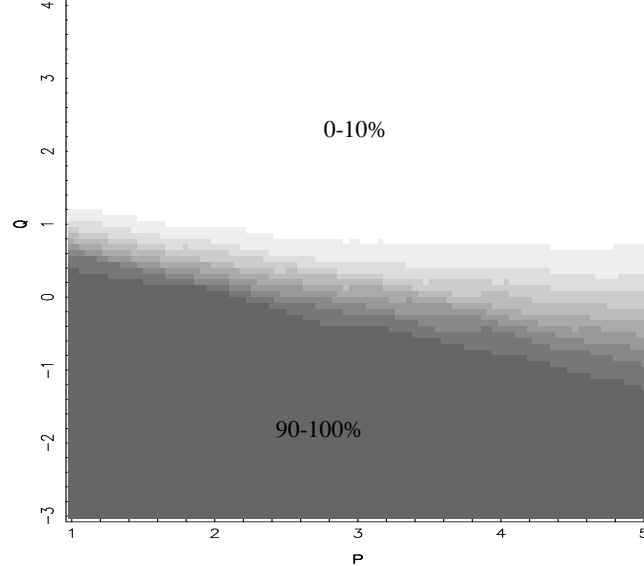
(b)  $z_t = 1.5$



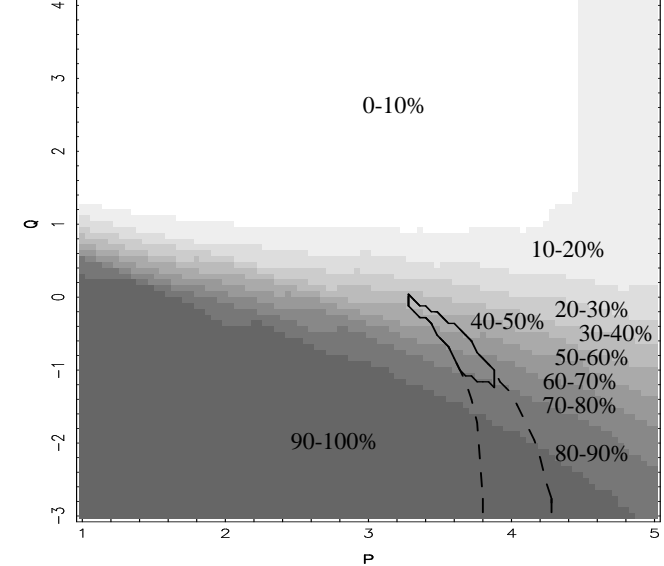
(c)  $z_t = 2.0$



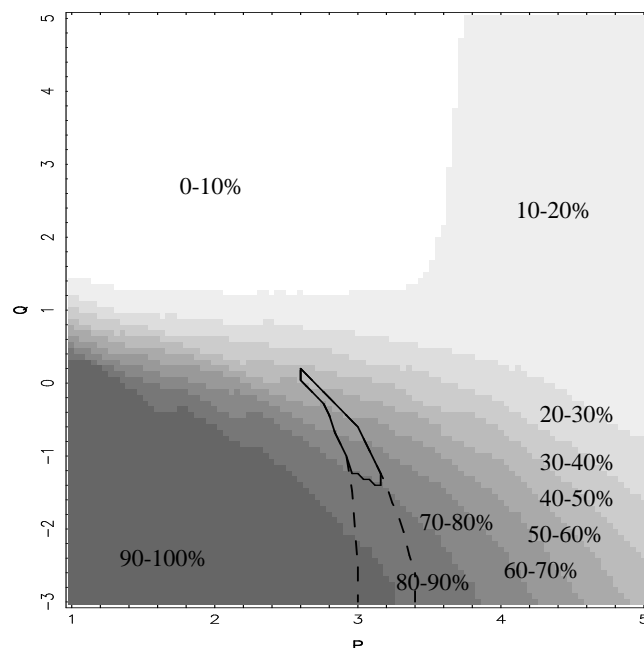
(d)  $z_t = 2.5$



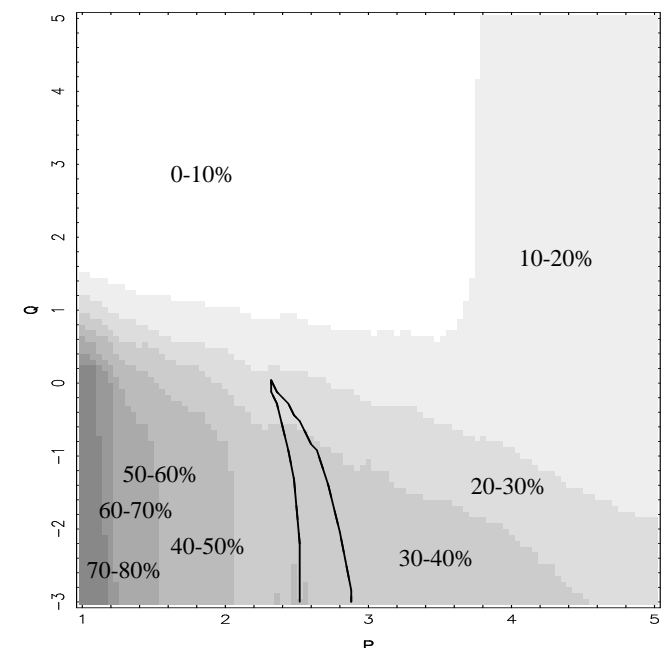
(a)  $z_t = 1.0$



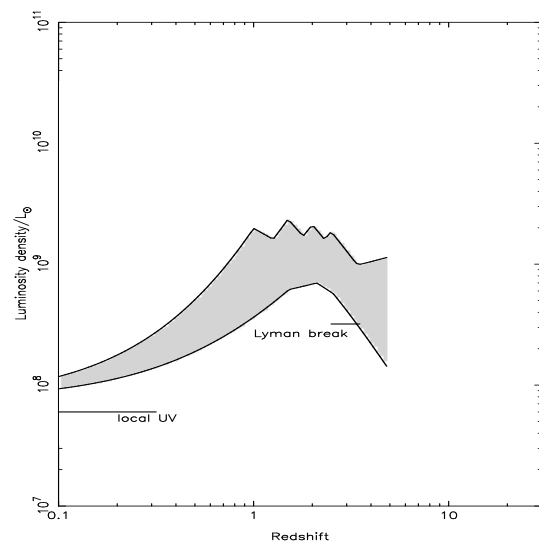
(b)  $z_t = 1.5$



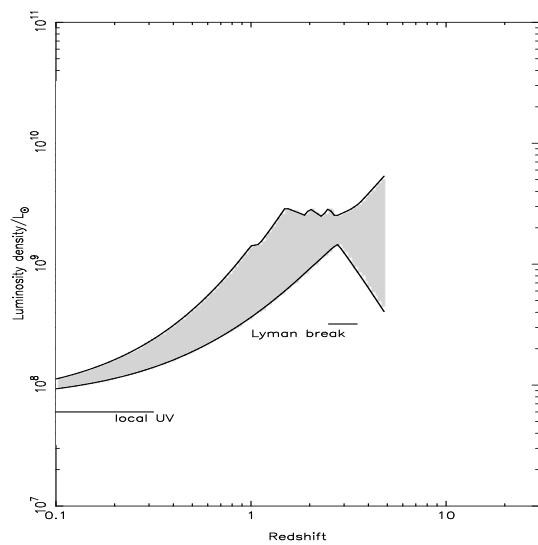
(c)  $z_t = 2.0$



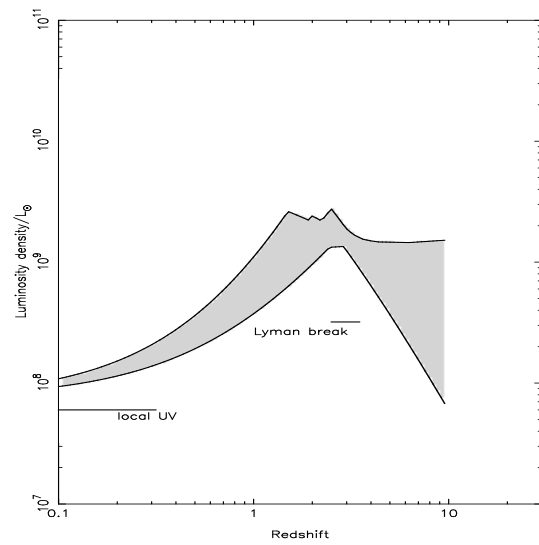
(d)  $z_t = 2.5$



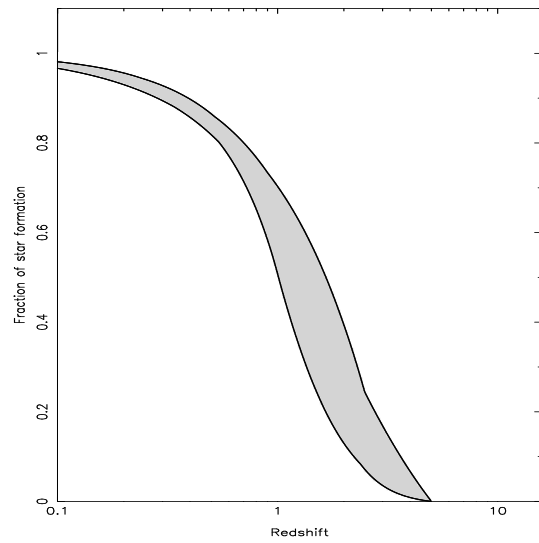
(a)  $\Omega_0 = 1$ ; no temperature evolution



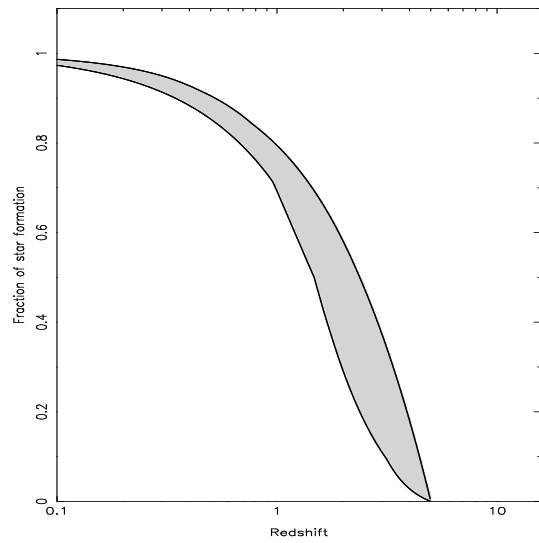
(b)  $\Omega_0 = 1$ ; temperature evolution;  $z_{max} = 5$



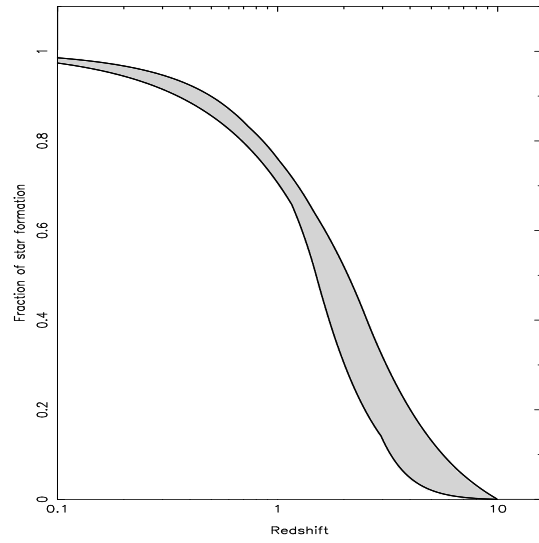
(c)  $\Omega_0 = 1$ ; temperature evolution;  $z_{max} = 10$



(a)  $\Omega_0 = 1$ ; no temperature evolution



(b)  $\Omega_0 = 1$ ; temperature evolution;  $z_{max} = 5$



(c)  $\Omega_0 = 1$ ; temperature evolution;  $z_{max} = 10$